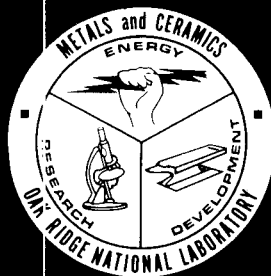




3 4456 0515935 1

*Cy.1*



# Inspection of High-Temperature Gas-Cooled Reactor Recycle Fuel

W. H. Pechin  
W. J. Lackey  
J. D. Sease  
W. P. Eatherly

OAK RIDGE NATIONAL LABORATORY  
CENTRAL RESEARCH LIBRARY  
DOCUMENT COLLECTION

## LIBRARY LOAN COPY

DO NOT TRANSFER TO ANOTHER PERSON

If you wish someone else to see this document, send in name with document and the library will arrange a loan.

# OAK RIDGE NATIONAL LABORATORY

OPERATED BY UNION CARBIDE CORPORATION FOR THE ENERGY RESEARCH AND DEVELOPMENT ADMINISTRATION

Printed in the United States of America. Available from  
National Technical Information Service  
U.S. Department of Commerce  
5285 Port Royal Road, Springfield, Virginia 22161  
Price: Printed Copy \$4.00; Microfiche \$3.00

This report was prepared as an account of work sponsored by the United States Government. Neither the United States nor the Energy Research and Development Administration/United States Nuclear Regulatory Commission, nor any of their employees, nor any of their contractors, subcontractors, or their employees, makes any warranty, express or implied, or assumes any legal liability or responsibility for the accuracy, completeness or usefulness of any information, apparatus, product or process disclosed, or represents that its use would not infringe privately owned rights.

ORNL-5165  
Distribution Category UC-77

Contract No. W-7405-eng-26

METALS AND CERAMICS DIVISION  
THORIUM UTILIZATION PROGRAM (189a 0H045)  
Refabrication Development – Task 300

INSPECTION OF HIGH-TEMPERATURE GAS-COOLED  
REACTOR RECYCLE FUEL

W. H. Pechin, W. J. Lackey, J. D. Sease, and W. P. Eatherly

Date Published: June 1977

OAK RIDGE NATIONAL LABORATORY  
Oak Ridge, Tennessee 37830  
operated by  
UNION CARBIDE CORPORATION  
for the  
ENERGY RESEARCH AND DEVELOPMENT ADMINISTRATION

LOCKHEED MARTIN ENERGY RESEARCH LIBRARIES



3 4456 0515935 1



## Contents

ABSTRACT .....	1
INTRODUCTION .....	1
KERNELS .....	3
COATED PARTICLES .....	4
Sampling .....	4
Particle Transfer .....	5
Coating Thickness and Particle Diameter .....	5
General Equations for Coating Density .....	10
As-Deposited Buffer Coating Density .....	12
LTI Coating Density .....	12
Buffer Coating Density After Deposition of the Low-Temperature Isotropic Layer .....	15
Silicon Carbide Coating Density .....	21
Particle Shape .....	21
Particle Strength .....	24
Cracked and Permeable Coatings .....	24
Kernel and Coating Microstructure .....	25
Coating Anisotropy .....	27
Uranium, Thorium, and Carbon Analysis .....	28
Impurity Analysis .....	31
FUEL RODS .....	31
Fuel Rod Transfer .....	31
Uranium Content .....	32
Actinide Homogeneity .....	32
FUEL ELEMENTS .....	33
Exposed Actinide .....	34
CONCLUSIONS AND RECOMMENDATIONS .....	34
APPENDIX A .....	35
ACKNOWLEDGMENTS .....	35



# INSPECTION OF HIGH-TEMPERATURE GAS-COOLED REACTOR RECYCLE FUEL

W. H. Pechin, W. J. Lackey, J. D. Sease, and W. P. Eatherly

## ABSTRACT

Inspection of recycle fuel for High Temperature Gas-Cooled Reactors (HTGRs) involves many operations which, because of the high radiation level associated with the presence of  $^{232}\text{U}$ , must be performed in shielded (5 cm of lead) glove boxes containing automated sample handling and analysis equipment. Equipment for obtaining representative fuel particle samples and for pneumatically transferring particles and fuel rods through long tubes has been developed. Schemes for cross checking inspection data were devised to determine the accuracy and precision of several analytical techniques as well as to detect occasional errors in analytical data. The density of the particle buffer coating layer was shown to increase significantly during deposition of the overlying pyrocarbon coating layer. A method was developed for measuring the final buffer density to an accuracy of about  $0.05 \text{ g/cm}^3$  while not requiring sampling at the buffer stage of the coating operation. Methods using high pressure mercury pycnometry were developed to measure both the amount of open porosity and the geometric density of low temperature isotropic (LTI) coatings. With this technique the LTI density can be measured with a precision of about  $0.01 \text{ g/cm}^3$ . A  $1500^\circ\text{C}$  gaseous chlorine leaching technique was shown to be useful for measuring defective Biso-coated particle fractions for both loose particles and particles bonded into fuel rods. An automated particle size analyzer suitable for glove box operation was developed with the capability for measuring particles at the rate of 1500 per min. Successful techniques for measuring particle shape and strength were also developed.

---

## INTRODUCTION

High-Temperature Gas-Cooled Reactors<sup>1</sup> (HTGRs) have the potential for supplying process heat and, if fuel recycle capability is established, HTGRs will provide improved fuel utilization when used to produce electricity. The HTGR fuel cycle begins with  $^{232}\text{Th}$  and  $^{235}\text{U}$ . As a result of neutron capture and subsequent radioactive decay, some  $^{232}\text{Th}$  is converted to  $^{233}\text{U}$ . The fuel recycling process consists of separating the bred  $^{233}\text{U}$  from the fission products and refabricating the  $^{233}\text{U}$  into fuel. This paper describes the quality control tests required for the refabrication of HTGR fuel.

Quality control tests for HTGR fuel have been under development for 15 years as part of the national HTGR recycle development program.<sup>2</sup> The major objective of this program is the development of commercial fuel recycle technology. Recently, a conceptual design of a refabrication pilot plant, including all required quality control functions, was completed.

The processing steps and product attributes (Fig. 1) that must be controlled during refabrication of HTGR fuel may be grouped in four basic categories: preparation of fuel kernels, application of multiple layers of pyrolytic carbon and silicon carbide, preparation of fuel rods, and loading of fuel rods into holes in graphite fuel elements.

Quality control of refabricated HTGR fuel presents a unique problem because of the presence of some  $^{232}\text{U}$ , which is not removed by chemical processing. The high-energy gamma radiation from the radioactive decay of daughter products of  $^{232}\text{U}$  requires that fabrication and quality control testing be performed in

---

1. H. B. Stewart, R. C. Dahlberg, W. V. Goeddel, D. B. Trauger, P. R. Kasten, and A. L. Lotts, "Utilization of the Thorium Cycle in the HTGR," *Peaceful Uses of Atomic Energy, Proc. 4th Int. Conf. Geneva, 1971*, United Nations, New York, and International Atomic Energy Agency, Vienna, 4: 433-47 (1972).

2. Oak Ridge National Laboratory, Gulf General Atomic, and Idaho Chemical Processing Plant, *National HTGR Fuel Recycle Development Plan*, ORNL-4702, Rev. 1 (August 1973).

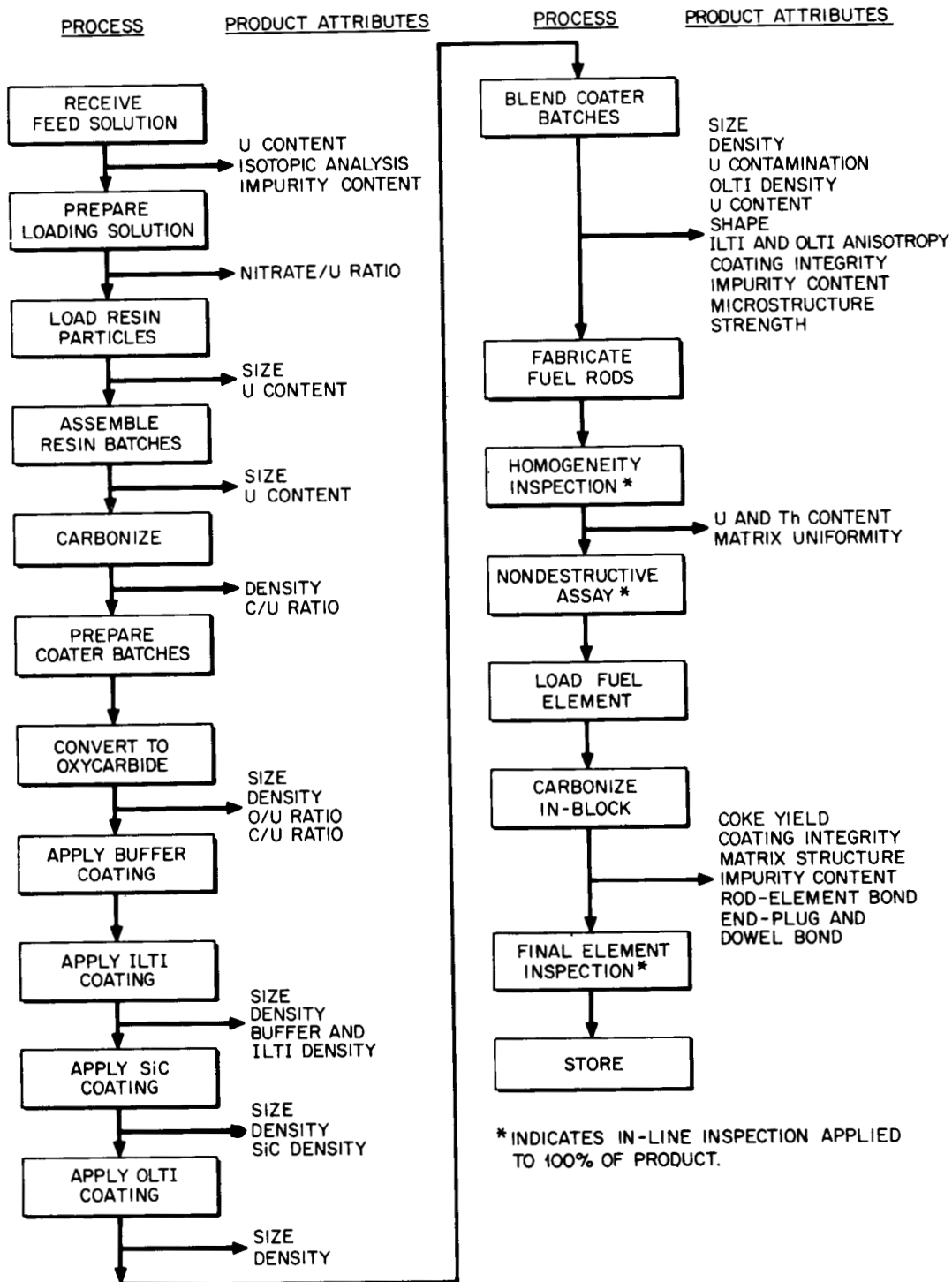


Fig. 1. Processing operations and inspection requirements for fabrication of recycle HTGR fuel.

shielded facilities. On-line inspection equipment must be located in the refabrication hot cell behind several feet of concrete. Calculations of personnel radiation exposure levels, a portion of which is summarized in Table 1, show that shielded (5 cm of lead) glove boxes are required for off-line quality control testing of typical fuel even when the sample size is limited to 0.5 g uranium. Automated sample handling and analysis equipment is required since samples cannot be manually handled. The fuel also has a high alpha activity; the hazard level is closer to that of  $^{239}\text{Pu}$  than to that of  $^{235}\text{U}$  (Ref. 3,4). In some stages of the process, the fuel kernels are pyrophoric and must be kept in an inert atmosphere to maintain the desired stoichiometry. Both on- and off-line quality control equipment is further complicated by the need for particles and fuel rods to be handled remotely.

### KERNELS

The kernel or fuel bearing portion of HTGR fuel particles can be an actinide oxide, a carbide, or a mixture of the two. The reference recycle fertile kernel is a 500- $\mu\text{m}$ -diam  $\text{ThO}_2$  microsphere.<sup>5,6</sup> The reference fissile kernel is a mixture of  $\text{UO}_2$ ,  $\text{U}(\text{C},\text{O})$ , and  $\text{UC}_2$  finely dispersed in a carbon matrix. The fissile kernels are obtained by loading<sup>7</sup> uranyl ions onto microspheres of weak acid ion exchange resin\* which are subsequently carbonized and heated in a fluidized bed to 1550–1800°C to convert the desired

\*Rohm and Haas IRC-72 or Diamond Shamrock C-464 resins are used.

3. J. E. Till, *A Comparison of the Potential Radiological Impact of Recycle  $^{233}\text{U}$  HTGR Fuel and LMFBR Plutonium Fuel Released to the Environment*, ORNL-TM-4768 (January 1975).

4. J. E. Till, *Assessment of the Radiological Impact of  $^{233}\text{U}$  and Daughters in Recycled  $^{233}\text{U}$  HTGR Fuel*, ORNL-TM-5049 (February 1976).

5. P. A. Haas, *Process Requirements for Preparing  $\text{ThO}_2$  Spheres by the ORNL-Sol-Gel Process*, ORNL-TM-3978 (December 1972).

6. P. A. Haas and W. J. Lackey, *Improved Size Uniformity of Sol-Gel Spheres by Imposing a Vibration on the Sol in Dispersion Nozzles*, ORNL-TM-4094 (May 1973).

7. P. A. Haas, *HTGR Fuel Development: Loading of Uranium on Carboxylic-Acid Cation Exchange Resins Using Solvent Extraction of Nitrate*, ORNL-TM-4955 (September 1975).

Table 1. Dose rates for a 1-g source of  $^{233}\text{U}$  with 500 ppm  $^{232}\text{U}$

Distance from source point to dose point (cm)	Dose rate (mrem/hr)			
	Days since separation from $^{232}\text{U}$ daughter products			
	30	60	90	180
<i>Without shielding</i>				
1	2,203	4,444	7,407	14,605
2	551	1,112	1,854	3,655
5	88.3	178	297	585
10	22.1	44.5	74.2	146
20	5.52	11.1	18.6	36.6
35	1.80	3.64	6.06	12.0
50	0.88	1.78	2.97	5.86
100	0.22	0.45	0.74	1.47
<i>Through 5 cm Pb</i>				
5.2	7.41	14.9	24.9	49.1
10.0	2.00	4.04	6.73	13.3
20.0	0.50	1.01	1.68	3.32
35.0	0.164	0.33	0.55	1.08
50.0	0.080	0.162	0.27	0.53

fraction of  $\text{UO}_2$  to carbide.<sup>8</sup> Important attributes of the kernels which must be controlled are size, shape, density, actinide and impurity content, and in the case of the resin-derived kernels, carbon and oxygen content. The kernels must also be capable of withstanding the thermal shock of being dropped into a hot coating furnace. The techniques required for particle characterization are discussed in the next section.

### COATED PARTICLES

The fertile  $\text{ThO}_2$  kernel is coated with two layers (Biso coating) which consist of a porous carbon buffer layer and a dense carbon outer layer commonly called a low temperature isotropic (LTI) coating (Fig. 2). An important function of the buffer coating is to provide space to accommodate kernel swelling and released fission gases. Therefore, the coating density and thickness must be controlled. The function of the LTI layer is to retain fission products. Therefore, its strength and ability to resist diffusion of gaseous and solid fission products is of concern. The fissile particle coating is referred to as the Triso design. It has two layers similar to those of the Biso coating with additional layers are SiC and high density carbon (LTI). The most important layer is the SiC which provides greater retention of fission products, particularly the solid fission products, than does the LTI layer in the Biso-coating design. All coatings are deposited in a batch process using high temperature fluidized beds at temperatures up to  $1600^\circ\text{C}$ . Thermal decomposition of hydrocarbons such as  $\text{C}_2\text{H}_2$  and  $\text{C}_3\text{H}_6$  produces the carbon coatings; the SiC is deposited by decomposition of  $\text{CH}_3\text{Cl}_3\text{Si}$  in the presence of hydrogen.

### Sampling

Particle-to-particle variations in size and density cause extensive segregation within a container of kernels or coated particles; therefore all samples must be obtained in such a way as to be truly representa-

8. D. R. Johnson, W. J. Lackey, and J. D. Sease, *The Effects of Processing Variables on HTGR Fuel Kernels Fabricated from Uranium-Loaded Cation-Exchange Resin*, ORNL-TM-4989 (August 1975).

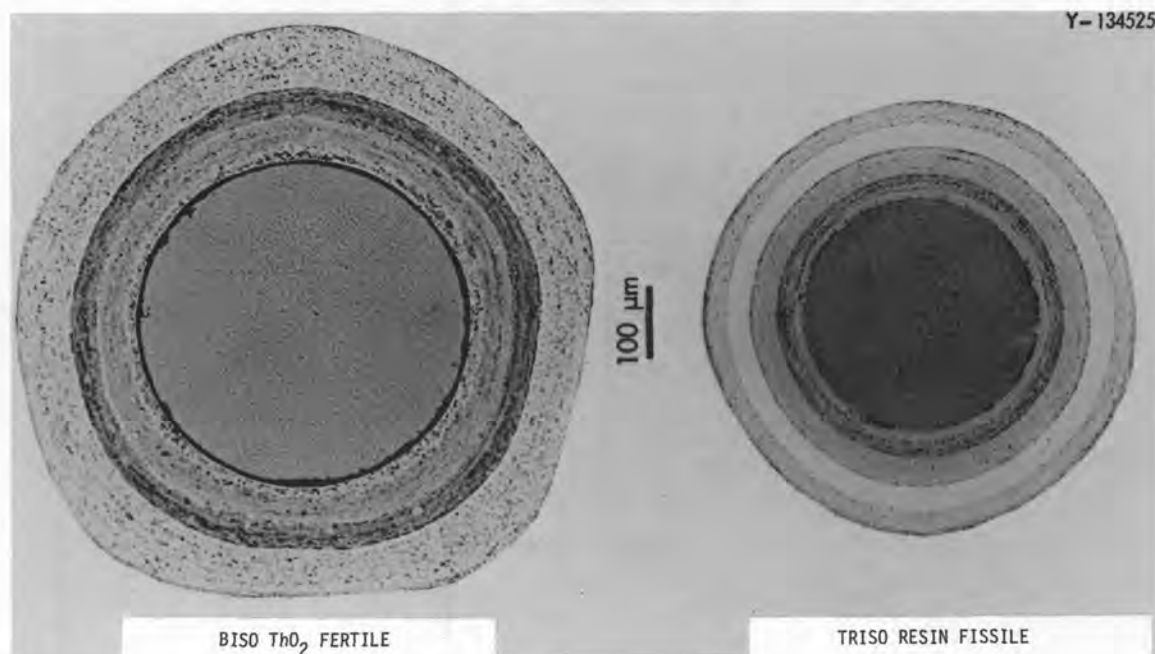


Fig. 2. Reference recycle fertile and fissile fuel particles.

tive. One such method using a two-way riffler has been successful in laboratory studies. For remote sampling two types of conical splitters have been developed which contain no moving parts and work satisfactorily. One type has ten conical stages with each stage splitting out one-half of the material and passing it on to the next stage (Fig. 3). The use of ten stages gives a sample of  $1/2^{10}$  or  $1/1024$  of the batch. A second sampler has three stages, each of which splits  $1/10$  of the batch yielding a sample which is  $1/1000$  of the initial batch (Fig. 4). In designing either type of sampler it is important that each stage combines a number of fractions obtained from diametrically opposite locations on the cone. In the first design the periphery of each conical stage was divided into eight segments with four alternate segments used to make up the sample. With the second type sampler the sample stream for each stage was obtained by combining 12 fractions. Extreme care must be taken to prevent particles which have already been diverted to the non-sample stream from bouncing back into the stream feeding a subsequent stage of the sampler. Also, particles must be carefully prevented from falling too far before their fall is interrupted; otherwise, weak particles, such as buffer coated material, will crack. Results show that both devices yield a representative sample while a grab sample is biased (Fig. 5).

### Particle Transfer

Numerous small samples of particles, some of which are pyrophoric, must be transported from the hot cell to a glove box inspection line. Feasibility has been demonstrated in an experimental test loop by vacuum transferring unencapsulated kernels and coated particles a distance of 55 m (180 ft) through 6.4-mm ( $1/4$ -in.) tubing with a pressure differential of 44 kPa (13 in. of mercury). Particle velocities are typically 15 m/sec (50 fps) and particle recovery was 100% with individual particles being transferred and collected as efficiently as several thousand particles. The system uses a cyclone separator to receive the particles and isolation valves to provide a vacuum lock between the transfer line and the hot cell and glove box atmospheres.

### Coating Thickness and Particle Diameter

Coating thickness and particle diameter are routinely measured by microscopic examination of high resolution x-radiographs<sup>9</sup> of particles (Fig. 6). A computerized scheme is used for reading microradiographs. The digital output from a filar eyepiece is immediately processed and printed by a small computer. Individual values, averages, standard deviations and other statistics are obtained for various coating thicknesses and particle diameters at different stages of coating.

The coating thickness or diameter of a particular particle can be made to an accuracy approaching 1  $\mu\text{m}$ . However, the particle-to-particle variation in coating thickness and diameter causes a larger uncertainty to be associated with the average values which characterize a particle batch. For example, if the standard deviation for the particle diameter distribution is 30  $\mu\text{m}$ , then the 95% confidence interval for the mean of 50 diameter measurements will be  $\pm 8.5 \mu\text{m}$ . The uncertainty is still  $\pm 4.3 \mu\text{m}$  for 200 measurements.

More precise and rapid particle diameter measurements can be obtained with a particle size analyzer which has been developed over the past several years and is in routine operation. In addition to measuring diameter the analyzer counts the number of particles per unit mass. This is useful in characterizing several particle parameters as well as for material accountability. This device is expected to be the major source of

---

9. R. W. McClung, *Studies in Contact Microradiography*, ORNL-3511 (October 1963).

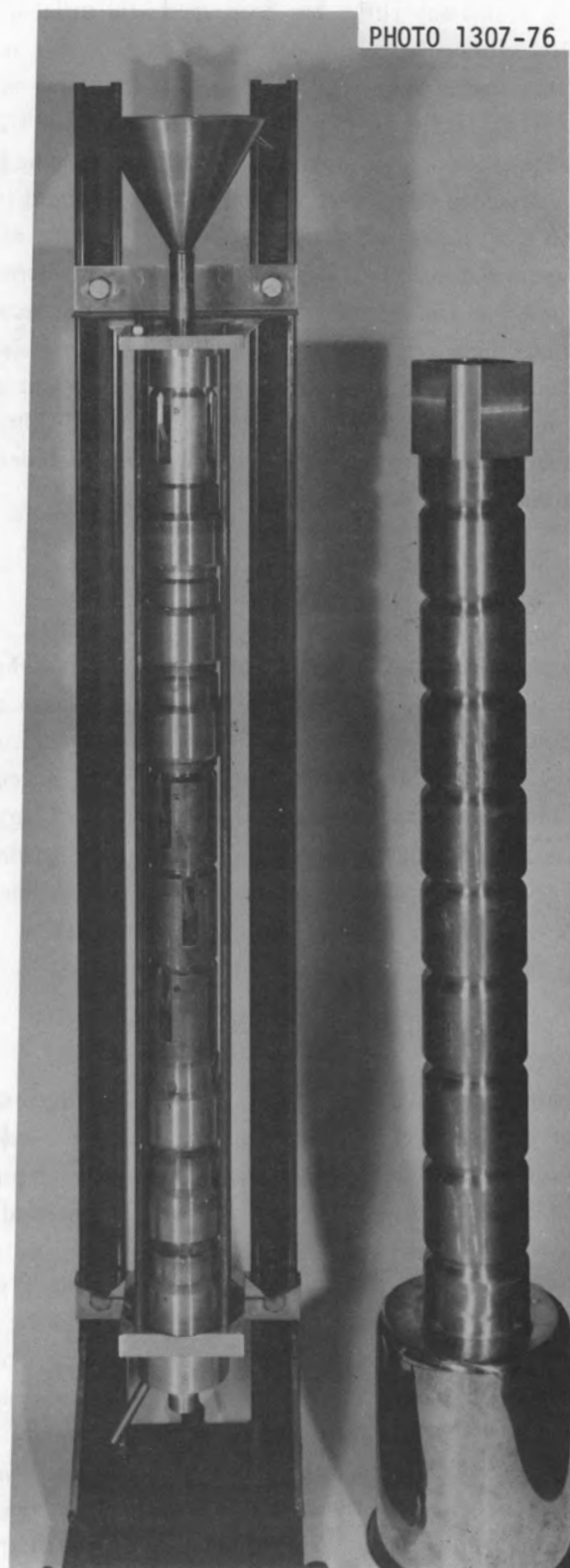


**Fig. 3. Ten-stage particle sampler.** In practice, the shell located to the right of the sampler is slid over the sampler and the restrictions in the shell prevent particles from bouncing back into the sample stream. The restrictions also interrupt the particle fall and thus prevent particle breakage.

PHOTO 2897-75

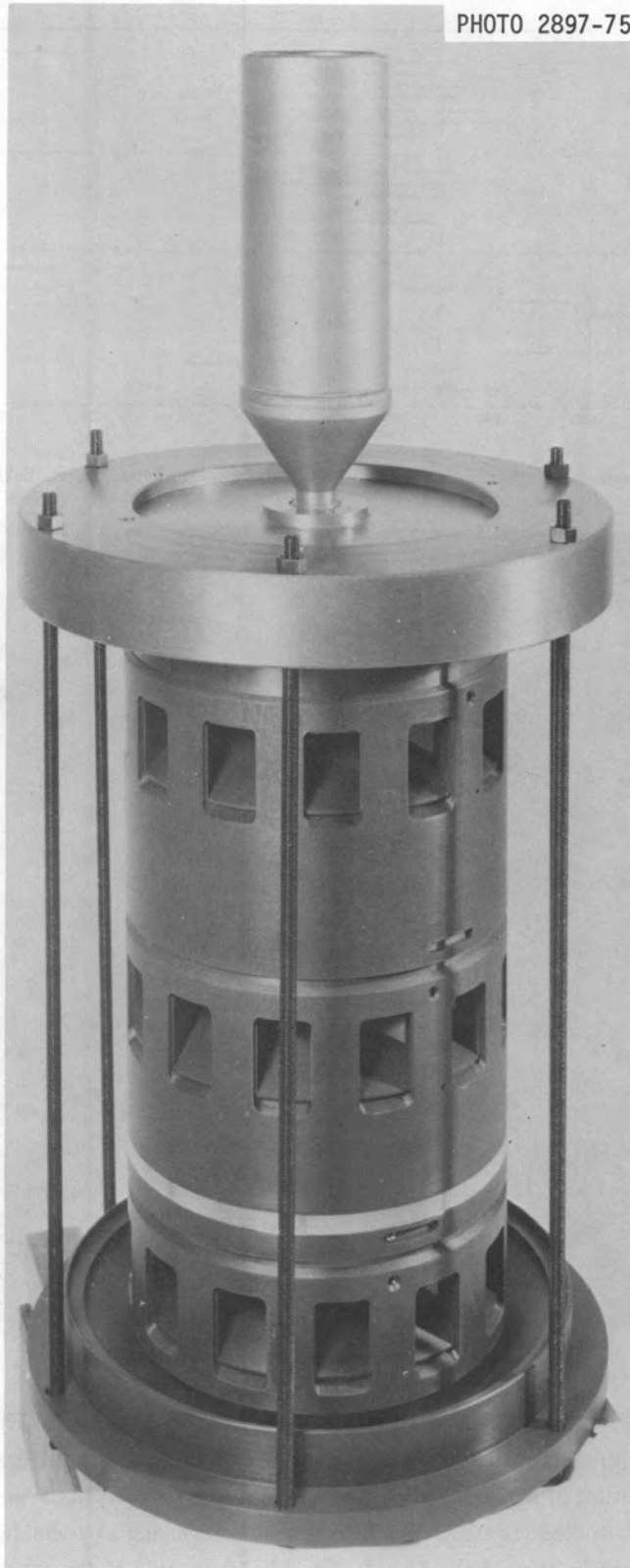


Fig. 4. Three-stage particle sampler. Shields, which are not shown, are placed around the bottom two stages to minimize particle bounding and to lower the particle velocity.

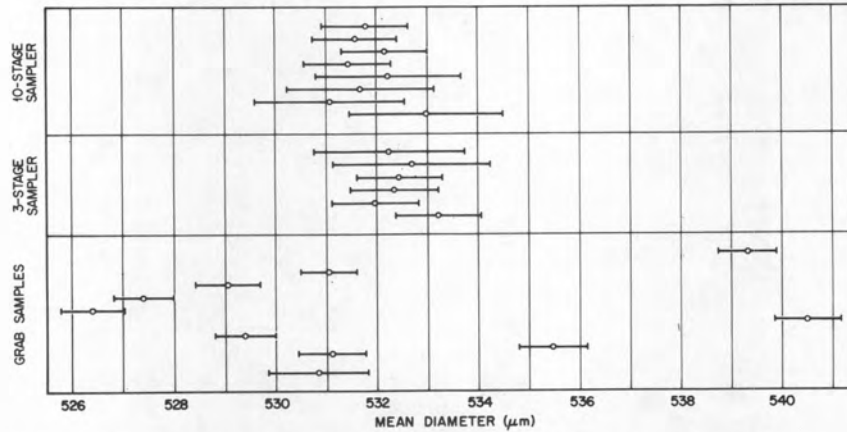


Fig. 5. Particle diameter distribution for split and grab samples of Biso-coated  $\text{ThO}_2$  particles.

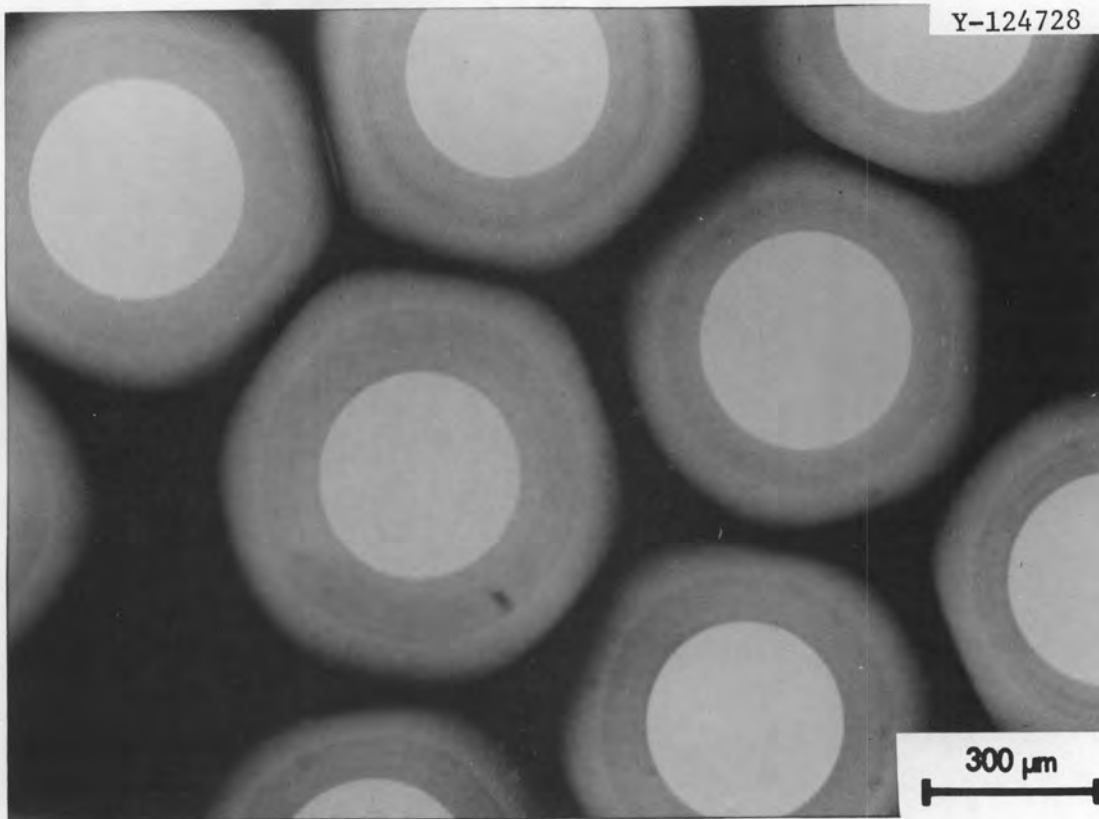


Fig. 6. Micro x-radiograph of Biso-coated  $\text{ThO}_2$  (75X).

process control data for particle coating operations of future refabrication plants. The unit (Fig. 7) operates using the light blockage principle; that is, as a particle passes through a light beam its shadow causes a decrease in the current output of a photodiode proportional to the cross-sectional area of the particle.

A Schottky barrier photodiode is used as the light detector, receiving a parallel homogeneous light beam from a high intensity light-emitting diode (LED). The LED is located at the focal point of a 1-cm-focal-length converging lens which provides a uniform light field across the face of the photodiode. After signal conditioning which includes analog-to-digital conversion the signal is recorded in one of 1024 channels of a

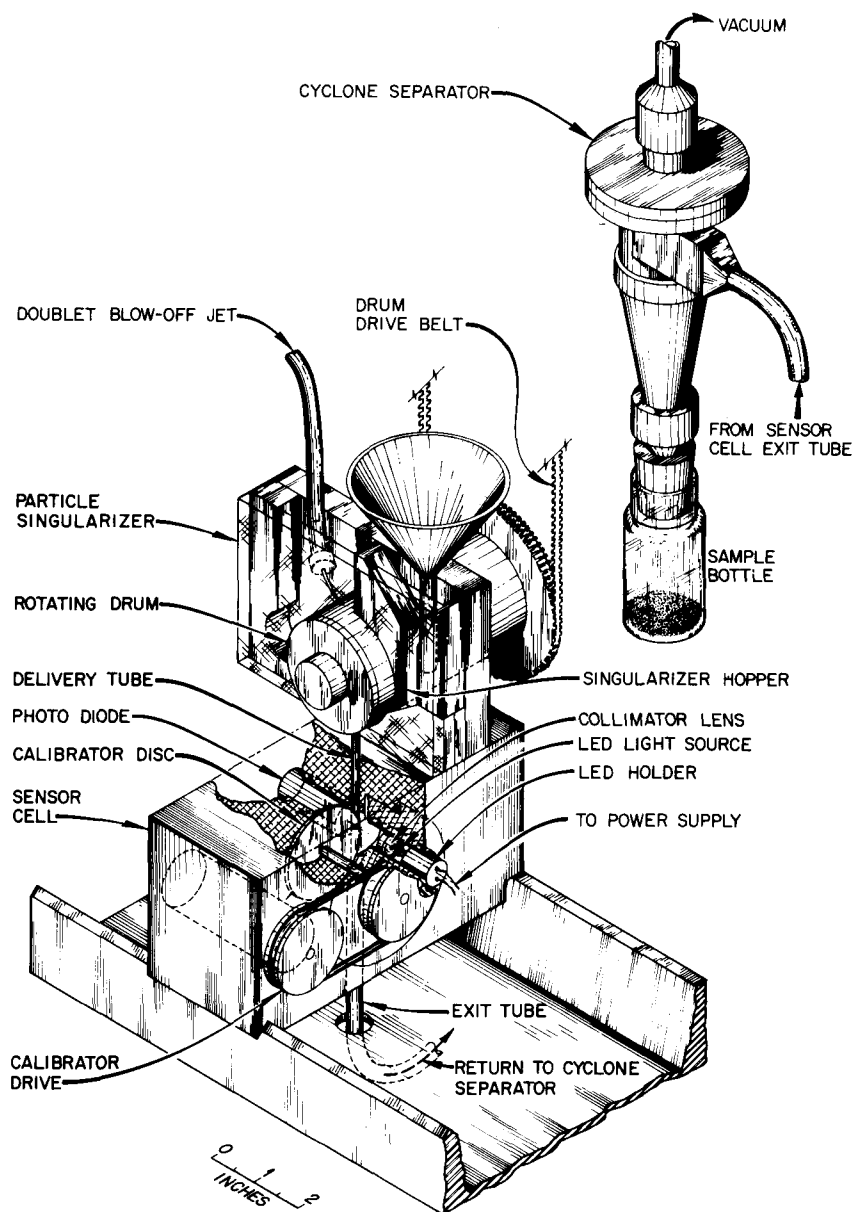


Fig. 7. Particle size analyzer.

pulse height analyzer. An important component is the particle singularizer (Fig. 7) which ensures that only a single particle is in the light beam at any one time, thus ensuring an accurate count. The singularizer uses a rotating evacuated drum to pick up particles individually on holes in the drum. As each hole reaches the proper position with respect to the analyzer delivery tube, an air jet positioned inside the drum dislodges the particle from the hole and drives it into the delivery tube. Particles can be measured at a rate of 1500 per min.

The particle size analyzer is calibrated in less than 5 min with a set of high-precision steel spheres of four sizes ranging from 380 to 800  $\mu\text{m}$ . A secondary calibration standard permits upgrading the calibration curves between sample runs. Six wires of different diameters protrude radially from a disk hub and

interrupts the light beam, creating pulses similar to those made by the coated particles. With this secondary standard a calibration check can be completed in 5 to 10 sec.

Nearly spherical steel microspheres produce size distributions with standard deviations of  $<1 \mu\text{m}$  when a single particle is recirculated 200 times. In contrast, the faceted coated particles characteristically yield standard deviations of 3 to 7  $\mu\text{m}$  for a single particle recirculated 200 times. Reproducibility of the results obtained with the analyzer has been excellent. The 95% confidence interval about the mean diameter is typically about 2  $\mu\text{m}$  for a sample of coated particles (Fig. 5). The counting efficiency for a clean sample is essentially 100%. These characteristics along with the fast turnaround time have made the particle size analyzer valuable for use in coated particle equipment and process development. An example of the utility of the particle size analyzer is the particle diameter distributions of Fig. 5.

### General Equations for Coating Density

Early work in measuring buffer and LTI coating densities centered around use of three primary pieces of information. These are: (1) the total coating weight, (2) the particle density after coating, and (3) the particle diameter and kernel diameter. Coating weight is measured by burning the carbon off the kernel; particle density is measured by mercury pycnometry; and particle and kernel diameters are determined by high resolution x-radiography of a sample of 50 particles. Any two of the three primary pieces of information may be used to calculate coating density; thus three combinations or equations exist. These three equations for calculating the density of the  $n$ th coating are easily derived by performing mass and volume balances and are as follows:

from particle density and burnoff,

$$\rho_1 = \frac{W - W'}{(W + 1)/\rho_p - (W' + 1)/\rho'_p} \quad (1)$$

from burnoff and radiograph,

$$\rho_2 = \frac{\rho_K (W - W')}{V - V'} \quad (2)$$

and from particle density and radiograph,

$$\rho_3 = \frac{\rho_p (V + 1) - \rho'_p (V' + 1)}{V - V'} \quad (3)$$

where

$$\rho_1, \rho_2, \rho_3 = \text{coating density, g/cm}^3$$

$$\rho_K = \text{kernel density, g/cm}^3$$

$$\rho_p = \text{particle density, g/cm}^3$$

$W$  = weight of coating relative to the kernel, g/g

$V$  = volume of coating relative to the kernel,  $\text{cm}^3/\text{cm}^3$

Primed quantities are values before the coating run; unprimed quantities are values after the run.

The value of  $V$  is determined from radiographic measurements of the diameter of the particle ( $D_p$ ) and kernel ( $D_K$ ). By calculating the ratio  $(D_p/D_K)^3$  for each of 50 particles and averaging the ratios, the  $V$  is computed using:

$$V = \left( \frac{D_p}{D_K} \right)^3 - 1. \quad (4)$$

Experience has shown that Equation (1), which is based on particle density and burnoff, is the most precise of the three. The precision of  $V$  which appears in the other two equations is controlled by the standard deviation of the ratio  $D_p/D_K$  among particles of the batch and by the number of particles measured. Equation (2) is not very sensitive to statistical variation in the value of  $V$  while Eq. (3) is virtually worthless because of its sensitivity to the variation inherent in  $V$ .

The first two methods using Eqs. (1) and (2) are cross-checked by comparing results averaged over a series of buffer coating runs. The accuracy of the radiographic measurements is maintained by calibrating the eyepiece against stage micrometers. The precision of the coating weight as determined by burnoff and the precision of the density determination which is done with a mercury pycnometer are checked by analyses of duplicate samples. Obtaining representative samples by careful riffing techniques is of the utmost importance. Usually the average difference between duplicate burnoff samples is 0.06%. Samples are burned in screen-covered platinum boats at 900°C. One important key to obtaining precise and accurate results was the addition of an oxygen purge to the furnace atmosphere to ensure complete combustion. A study of the effect of sample size on particle density values obtained by mercury pycnometry showed that by increasing the sample size from 0.5 to 2  $\text{cm}^3$  the relative standard deviation was reduced from 0.4 to 0.1%. The 2  $\text{cm}^3$  sample is now routinely used. Also, 1.72 MPa (250 psi) mercury is used to fill the necks formed between adjacent particles but with negligible penetration of the coating.

Equations (1) through (3) are always valid for as deposited buffer coatings and are also valid for LTI coatings where the LTI layer is deposited over a nonpermeable substrate as is the case for the outer LTI layer of particles of the Triso design. However, we have repeatedly observed if an LTI coating is deposited on a buffer-coated substrate, some of the carbon deposited during the LTI coating step infiltrates the open pores of the buffer coating. As a result equations (1) and (2) yield erroneously high values for the LTI density since some of the carbon detected during the burnoff analysis is located within the buffer layer. The interface between the buffer and LTI layers remains very distinct as verified by metallographic observation; thus it is appropriate to associate the infiltrated carbon with the buffer rather than the LTI layer. For this reason, the above equations for calculating LTI density are not used if the substrate is a buffer coating or even a so-called "sealed" buffer coating. The conventional thin sealer layer (up to 5- $\mu\text{m}$  thick) has been found to be ineffective in preventing infiltration of the buffer layer during LTI coating and use of the sealer has been stopped. Infiltration alters the density and open pore volume of the buffer coating compared to the as-deposited buffer coating prior to deposition of the LTI layer. Therefore two values for buffer density are usually reported. One value is for the buffer prior to LTI deposition. The second value is the buffer density after LTI deposition and is obtained by dividing the mass of the as deposited buffer plus the mass of carbon which infiltrated the buffer by the volume of the as-deposited buffer layer. Details of the methods for calculating both buffer density values are presented below.

### As-Deposited Buffer Coating Density

Equation (1) is currently best for accurately calculating the density of as-deposited buffer coatings, i.e. the buffer density before deposition of the LTI layer. When the coating densities for 12 different buffer coating runs were each analyzed in duplicate using Eq. (1), the average difference in the duplicate values was only 0.007 g/cm<sup>3</sup> (Table 2). While not as precise, Eq. (2) is also useful for calculating densities of as-deposited buffer coatings. One method for checking the accuracy of the analytical data is to compare buffer coating densities calculated by the two equations (Table 1). For 31 buffer coating runs compared in this manner, the absolute difference between coating density values obtained with Eqs. (1) and (2) averaged 0.027 g/cm<sup>3</sup>. If all of the difference is assigned to the radiographic measurement, then this difference would correspond to an error in the particle-to-kernel diameter ratio of <0.8%. While this is larger than the precisions quoted above for the burnoff and density determinations, it is still sufficiently accurate to give a good cross check on the data and to improve our confidence in the calculated coating density. Such cross checking of the data is easily computerized and is highly recommended.

### LTI Coating Density

As discussed, Eq. (1) is valid for calculating the geometric (bulk) density of LTI coatings provided the substrate is impermeable. For the LTI coating of Biso-coated particles and the inner LTI of Triso-coated particles the substrate is permeable; thus, an alternative technique has been developed to obtain the geometric density of the LTI layer. This new technique makes combined use of the LTI layer's open porosity fraction and the coating density obtained by the gradient column<sup>10,11</sup> or sink-float<sup>12</sup> techniques. The liquid immersion techniques for measuring the density of LTI coating fragments do not measure

10. G. Oster and M. Yamamoto, "Density Gradient Techniques," *Chem. Rev.* 63: 257–68 (1963).

11. D. C. Canada and W. R. Laing, "Use of a Density Gradient Column to Measure the Density of Microspheres," *Anal. Chem.* 39: 691–92 (1967).

12. Manfred Gordon and Iain A. Macnab, "A New Diffusion Gradient Method for Thermal Expansion Studies with Application to Polystyrene," *Trans. Faraday Soc.*, 49: 31–39 (1953).

Table 2. As-deposited buffer coating density values calculated using Eq. (1) and (2) for 12 buffer coating runs

Run	Buffer density from Eq. (1) (g/cm <sup>3</sup> )	Duplicate Measurement using Eq. (1) (g/cm <sup>3</sup> )	Average for Eq. (1) (g/cm <sup>3</sup> )	Buffer density from Eq. (2) (g/cm <sup>3</sup> )
A-273	1.150	1.144	1.147	1.175
A-275	1.138	1.123	1.130	1.033
A-277	1.121	1.131	1.126	1.079
A-278	1.133	1.132	1.133	1.111
A-279	1.124	1.139	1.132	1.139
A-280	1.125	1.124	1.125	1.113
A-281	1.133	1.126	1.130	1.167
A-282	1.149	1.133	1.141	1.149
A-283	1.131	1.130	1.130	1.117
A-284	1.135	1.140	1.138	1.106
A-285	1.138	1.132	1.135	1.186
A-286	1.137	1.138	1.138	1.227
Averages	1.134	1.133	1.134	1.134

geometric density of the LTI coating because the liquid penetrates and fills all open pores. Thus the observed immersion density ( $\rho_O$ ) is the ratio of the mass ( $m$ ) of the LTI fragment divided by the volume of the fragment excluding the volume of open pores – that is,

$$\rho_O = m/(V - PV), \quad (5)$$

where  $V$  is the bulk volume of the coating and  $P$  is the fraction of the LTI volume which is open pores.

The bulk or geometric density ( $\rho_C$ ) of the LTI coating is defined as the mass of the coating divided by its bulk volume – that is,

$$\rho_C = m/V. \quad (6)$$

Solving Eqs. (5) and (6) for  $m$  and equating them yields the corrected immersion density (geometric density) in terms of the observed immersion density and fraction of open porosity:

$$\rho_C = \rho_O (1 - P). \quad (7)$$

Thus, Eq. (7) can be used to obtain the geometric density of the LTI layer from the observed immersion density provided the pore volume of the LTI layer is known. Fortunately, it is easy enough to measure this pore volume by high pressure mercury pycnometry. For either Biso-coated or Triso-coated particles the difference in densities determined by low and high pressure mercury pycnometry is related to the fraction of the outer coating volume that is open pores.

The mercury pycnometry data is used in the following manner: For a unit mass of particles the bulk particle volume is given by  $\frac{1}{\rho_L}$ , where  $\rho_L$  is the particle density as determined by low pressure (1.72 MPa or 250 psi) mercury pycnometry. Similarly, the particle volume excluding the open pores in the outer coating layer which are filled by high pressure (103 MPa or 15,000 psi) mercury is given by  $1/\rho_H$ , where  $\rho_H$  is the particle density determined by high pressure mercury pycnometry. The difference in these two particle volumes ( $1/\rho_L - 1/\rho_H$ ) is the volume of open pores per unit *mass* of particles. It follows that multiplying this term by  $\rho_L$  gives the volume of open pores ( $V_P$ ) per unit *volume* of particles  $\left(\frac{\pi}{6}D_L^3\right)$  – that is,

$$\frac{V_P}{\frac{\pi}{6}D_L^3} = \rho_L(1/\rho_L - 1/\rho_H) \quad (8)$$

where  $D_L$  is the diameter of the LTI coated particle.

For a Biso-coated particle the geometric volume of the particle is equal to the geometric volume of the buffer coated particle plus the geometric volume of the LTI coating – that is,

$$\frac{\pi}{6}D_L^3 = \frac{\pi}{6}D_B^3 + \frac{\pi}{6}(D_L^3 - D_B^3) \quad (9)$$

where  $D_B$  is the diameter of the buffer coated particle.

Solving Eqs. (8) and (9) for  $D_L^3$  and equating yields after simplification,

$$\frac{V_P}{\frac{\pi}{6}(D_L^3 - D_B^3)} = \frac{1 - \rho_L/\rho_H}{1 - 1/(D_L/D_B)^3} \quad (10)$$

The left side of Equation (10) is the fraction of the volume of the LTI layer which is open pores ( $P$ ) – thus,

$$P = \frac{1 - \rho_L/\rho_H}{1 - 1/(D_L/D_B)^3} \quad (11)$$

The immersion density is corrected by determining with Eq. (11) the open porosity fraction of the volume of the LTI layer and substituting this porosity value into Eq. (7). In practice the term  $(D_L/D_B)^3$  is obtained by summing the volume ratios – that is,  $\sum_{i=1}^n (D_{L_i}/D_{B_i})^3$ . However, simply dividing the average particle diameter by the average diameter of the buffer coated particle and cubing has been shown by numerous comparisons to be sufficiently accurate. Equation (11) also applies to the outer LTI layer of a Triso-coated particle, if  $D_L$  and  $D_B$  are replaced by the diameter of the Triso-coated particle and the diameter of the silicon carbide coated particle, respectively; and density values for the fully Triso-coated particle determined by low and high pressure pycnometry are used for  $\rho_L$  and  $\rho_H$ , respectively.

It is important to note that each analysis used to obtain the data to determine the fraction of open porosity and the corrected immersion density can be performed with samples of Biso-coated particles. In the case of the outer LTI layer all that is required is a sample of fully Triso-coated particles. In other words it is not necessary for purposes of obtaining the porosity and corrected immersion density to sample before the application of the LTI layer. This is an important consideration for a commercial production operation.

If sampling is done before application of the LTI layer, as is often done for research and development work, there is a second technique for calculating open porosity and thus the corrected immersion density. The second technique uses Eq. (1) which requires sampling of the substrate, or in the case of fully Triso coated particles, a riffled portion of particles is burned back to the SiC layer. Two LTI coating density values are calculated by substituting for  $\rho_P$  in Eq. (1) the particle density determined at low pressure and at high pressure, respectively. The ratio of the two calculated coating density values yields the fraction of the LTI layer which is open porosity:

$$P = 1 - \rho_{1(1.72 \text{ MPa})} / \rho_{1(103 \text{ MPa})} \quad (12)$$

where  $\rho_{1(1.72 \text{ MPa})}$  is the LTI coating density calculated from Eq. (1) using the low pressure value for particle density, and  $\rho_{1(103 \text{ MPa})}$  is the LTI coating density calculated from Eq. (1) using the high pressure value for particle density.

Equation (12) is exact even when infiltration of the substrate occurs since the errors in  $\rho_{1(1.72 \text{ MPa})}$  and  $\rho_{1(103 \text{ MPa})}$  caused by infiltration exactly cancel in the ratio. The fraction porosity from Eq. (12) is used to determine the corrected gradient density from Eq. (7).

These methods for calculating the geometric densities of LTI coatings were validated by the following experiment. Different LTI coating runs were made using impermeable  $\text{ThO}_2$  kernels as the substrate. The LTI density for each coating run was measured using several different techniques and compared. Since the substrate was impermeable Eq. (1) was used directly to very accurately obtain the geometric LTI layer density, and both methods for correcting the immersion density value were also applicable (Table 3). Values in the third column were calculated using Eq. (1) and are the most precise measure of the geometric density of the LTI layer. The fourth column was also obtained using Eq. (1) and a particle density value determined by high pressure mercury pycnometry. The resulting calculated coating density agrees with the observed immersion density values of column 2. This agreement is important since the comparison is an independent check on the accuracy and precision of the measurement of particle and kernel density, carbon content, and immersion density. The fifth and sixth columns give the fraction of the LTI volume which is open pores calculated using Eqs. (11) and (12), respectively. Columns 7 and 8 give the corrected immersion density obtained from Eq. (7) when used in conjunction with Eqs. (11) and (12), respectively. Values from the two methods of calculating corrected gradient density compare very favorably and are in good agreement with the geometric density values of column 3. This gives confidence in the procedures for calculating the corrected gradient density.

As can be observed metallographically, the outer portion (up to  $10 \mu\text{m}$ ) of an LTI coating is more porous than the remainder of the coating layer since this outer skeleton portion of the coating layer did not get infiltrated as much as would have occurred had the coating operation continued. The thickness of this outer porous region is essentially independent of the total LTI coating thickness and thus the difference in observed and corrected immersion density values is greatest for thin LTI coatings (Fig. 8). The observed immersion density was rather insensitive to a change in LTI deposition rate, whereas the corrected immersion density differed by a large amount for the two deposition rates (Fig. 8). This is an important difference and has been observed repeatedly for other coating process variables. Thus, the difference between observed and corrected immersion density is not fixed but depends on the details of the coating process. Both density values should be determined since a unique correlation between the two does not exist. Also the coating thickness, or better, the coating ID and OD should be reported.

Alternatively, the results of the high pressure mercury pycnometry analysis can be expressed in terms of the volume of open pores per unit mass of LTI coating; but this method is not recommended since the volume of pores per unit mass of coating can remain relatively constant while coating density, measured by observed and corrected immersion density, can simultaneously vary over a wide range.

#### **Buffer Coating Density After Deposition of the Low-Temperature Isotropic Layer**

As discussed, carbon infiltrates the buffer coating during deposition of the LTI layer and alters the density and volume available to accommodate fission gases and fuel swelling. Consequently two methods have been devised to measure the buffer density existing after LTI layer deposition. If sampling is performed both before and after LTI coating, then an equation based on burnoff and mercury density determinations can be used. If sampling is performed only after LTI coating, an alternate equation involving radiographic measurements is used.

First consider the derivation of the equation which does not require radiographic measurements. A carbon mass balance for the Biso-coated particle equates the total carbon content to the mass of carbon in the as-deposited buffer layer plus the mass of carbon infiltrating the buffer plus the mass of carbon in the LTI layer. The carbon mass balance based on a unit mass of kernel is:

$$W = W' + \Delta\rho(W'/\rho'_B) + \rho_C(W - W')/\rho_1 . \quad (13)$$

Table 3. Comparison of LTI coating density measurement techniques

Sample	Observed immersion density (g/cm <sup>3</sup> )	Eq. (1) using mercury pycnometer (1.72 MPa) and burnoff (g/cm <sup>3</sup> )	Eq. (1) using mercury pycnometer (103 MPa) and burnoff (g/cm <sup>3</sup> )	Fraction open porosity from Eq. (11)	Fraction open porosity from Eq. (12)	Corrected immersion density from Eqs. (7) and (11) (g/cm <sup>3</sup> )	Corrected immersion density from Eqs. (7) and (12) (g/cm <sup>3</sup> )
J-349	1.712	1.642	1.710	4.01	3.97	1.643	1.644
J-350	1.817	1.759	1.802	2.46	2.41	1.772	1.773
J-351	1.502	1.441	1.491	3.42	3.38	1.451	1.451
J-352	2.013	1.998	2.016	0.90	0.89	1.995	1.995
J-353	1.946	1.895	1.946	2.71	2.64	1.893	1.895
J-354	1.720	1.649	1.726	4.55	4.45	1.642	1.643
J-355	2.044	2.040	2.048	0.36	0.35	2.037	2.037
J-356	1.905	1.873	1.908	1.85	1.83	1.870	1.870
J-357	1.628	1.583	1.627	2.74	2.69	1.583	1.584
J-358	1.948	1.812	1.941	6.68	6.63	1.818	1.819

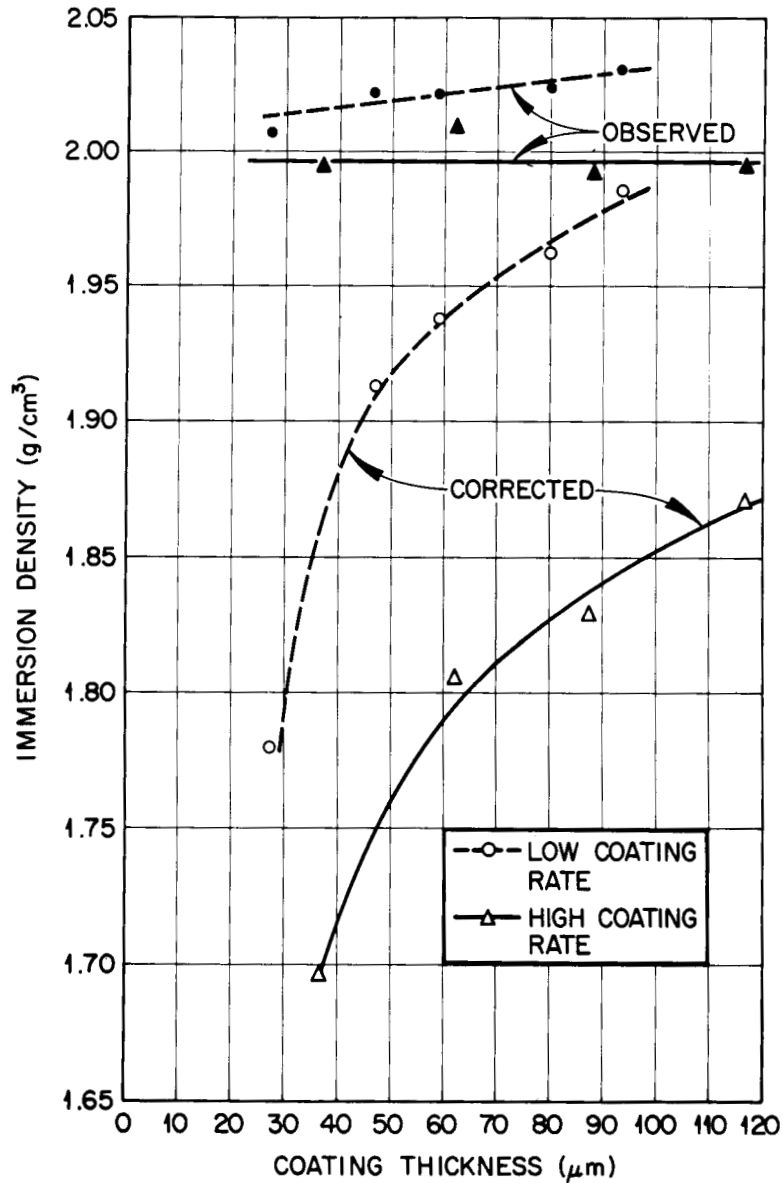


Fig. 8. Observed and corrected immersion density versus LTI coating thickness for low and high coating rate.

where:

$W$  and  $W'$  = the mass of carbon coating relative to the kernel mass after and before LTI coating, g/g;

$\Delta\rho$  = the mass of carbon that infiltrated the buffer layer per unit volume of buffer coating, g/cm<sup>3</sup>;

$\rho'_B$  = the buffer density before deposition of the LTI layer, g/cm<sup>3</sup>;

$\rho_C$  = the LTI layer corrected immersion density, g/cm<sup>3</sup>; and

$\rho_1$  = the value for the LTI layer density obtained by using the low pressure particle density from Eq. (1), g/cm<sup>3</sup>.

To aid in understanding the last two terms in Eq. (13) realize that multiplying  $\Delta\rho$  by  $W'/\rho'_B$  converts  $\Delta\rho$  to the basis of mass infiltrated per unit mass of kernel. The factor  $(W-W')/\rho_1$  is the volume of the LTI layer per unit mass of kernel and thus multiplying by the corrected LTI density ( $\rho_C$ ) gives the mass of LTI material per unit mass of kernel. Solving Eq. (13) for  $\Delta\rho$  gives:

$$\Delta\rho = \left(1 - \frac{\rho_C}{\rho_1}\right) \left(\frac{W}{W'} - 1\right) \rho'_B. \quad (14)$$

The buffer density after deposition of the LTI is now simply obtained by adding the mass infiltrated to the as-deposited buffer density – that is,

$$\rho_B = \rho'_B + \Delta\rho \quad (15)$$

Since only burnoff and mercury pycnometry density determinations are involved Equation (15) accurately yields the buffer density after deposition of the LTI layer. Attention is called to the fact that if the kernel contains carbon then  $W$  and  $W'$  of Eq. (14) are given by

$$\frac{1}{[1/(C_L - C_0 U_L/U_0)] - 1} \quad \text{and} \quad \frac{1}{[1/(C_B - C_0 U_B/U_0)] - 1}$$

where

$C_L$  = weight fraction carbon in the Biso-coated particle,

$C_0$  = weight fraction carbon in the kernel,

$U_L$  = weight fraction uranium or other actinide in the Biso-coated particle, and

$U_0$  = weight fraction uranium or other actinide in the kernel.

The alternate equation for calculating the infiltrated buffer density when sampling is performed only on the Biso-coated particles is derived by performing two mass balances. First, a total mass balance is made followed by a carbon mass balance. The total mass of the particle is equal to the sum of the masses of the kernel, buffer, and LTI coating. The mass of each component is equal to its volume multiplied by its density. Using the symbols defined in Appendix A, the total mass balance is given by:

$$\frac{\pi}{6} \rho_L D_L^3 = \frac{\pi}{6} \rho_K D_K^3 + \frac{\pi}{6} \rho_B (D_B^3 - D_K^3) + \frac{\pi}{6} \rho_C (D_L^3 - D_B^3) \quad (16)$$

Simplifying and solving for  $\rho_B$  gives:

$$\rho_B = \frac{\rho_L D_L^3 - \rho_C (D_L^3 - D_B^3) - \rho_K D_K^3}{D_B^3 - D_K^3} \quad (17)$$

Dividing numerator and denominator by  $D_K^3$  and setting  $R_1 = (D_B/D_K)^3$  and  $R_2 = (D_L/D_K)^3$  results in:

$$\rho_B = \frac{\rho_L R_2 - \rho_C (R_2 - R_1) - \rho_K}{R_1 - 1} \quad (18)$$

Equation (18) could be used to calculate the corrected buffer density, but the quantity  $(R_2 - R_1)$  is the difference of the two least precisely measurable parameters involved and therefore it is desirable to eliminate this quantity. Consider a Biso-coated particle containing a kernel which does not contain carbon, for example,  $\text{ThO}_2$  or  $\text{UO}_2$ . The mass of carbon in the coated particle is equal to the carbon in the buffer plus the carbon in the LTI. The carbon balance is given by:

$$\frac{\pi}{6} f \rho_L D_L^3 = \frac{\pi}{6} \rho_B (D_B^3 - D_K^3) + \frac{\pi}{6} \rho_C (D_L^3 - D_B^3) \quad (19)$$

or, after simplifying as before

$$\rho_B = \frac{f \rho_L R_2 - \rho_C (R_2 - R_1)}{R_1 - 1} \quad (20)$$

Combining Eqs. (20) and (22) yields:

$$f \rho_L R_2 - \rho_C (R_2 - R_1) = \rho_L R_2 - \rho_C (R_2 - R_1) - \rho_K \quad (21)$$

Solving for  $R_2$ ,

$$R_2 = \frac{\rho_K}{\rho_L (1 - f)} \quad (22)$$

Substituting Eq. (22) for  $R_2$  in Eq. (18) and simplifying gives the desired equation for corrected buffer density as follows:

$$\rho_B = \frac{\left\{ \rho_K / [\rho_L (1 - f)] \right\} (\rho_L - \rho_C) + \rho_C R_1 - \rho_K}{R_1 - 1} \quad (23)$$

When the kernel contains carbon as well as actinide,  $f$  in Eq. (23) is replaced by  $f = C_L - C_0 U_L / U_0$  where the symbols were previously defined.

Figure 9 shows the increases observed in buffer density during LTI coating. Note that infiltration depends on the LTI coating conditions: less infiltration was generally observed for higher LTI deposition temperatures.

Before these LTI runs a so-called "sealer" layer 2  $\mu\text{m}$  thick had been deposited over the buffer coating. Before application of the sealer the buffer density was about 1.1  $\text{g/cm}^3$ . After applying the sealer the density of the composite coating was 1.240  $\text{g/cm}^3$ ; and thus 1.240 must be added to each value in Fig. 9 to obtain the density of the buffer after applying the LTI layer. If the sealer had not been applied the values in Fig. 9 would be somewhat larger, but the final buffer densities would be about the same or slightly less. For the most severe infiltration encountered the buffer density increased from 0.67 to 1.51  $\text{g/cm}^3$  during LTI deposition.

One complicating factor enters into calculating both the corrected gradient density for the LTI coating and the buffer density after application of the LTI when the buffer coated particles are not sampled.

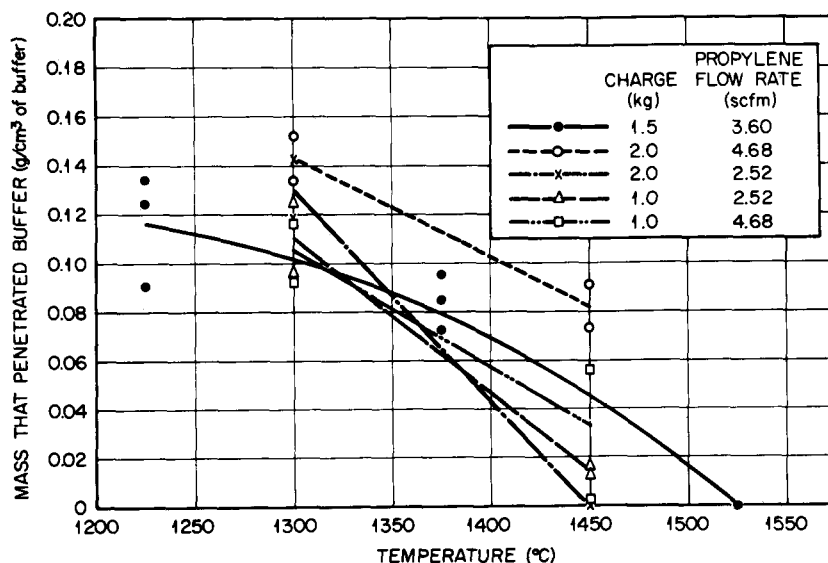


Fig. 9. Increase in buffer coating density caused by infiltration during the LTI coating operation.

Equations (11) and (23) contain diameter ratios whose measurement requires location of the buffer-LTI interface in an x-radiograph of Biso-coated particles. For Biso-coated particles the apparent location of this interface on a radiograph is actually several microns inside the true interface (the true interface being defined as the extremities of the buffer coated particles prior to LTI coating). By comparing the average buffer particle diameter as determined from a radiograph of buffer coated particles prior to LTI coating with the average buffer particle diameter as determined from a radiograph of particles from the same batch after LTI coating, the error associated with determination of the buffer-LTI interface can be determined. Usually the diameter difference is about  $8 \mu\text{m}$  for particles coated using a porous plate gas distributor and somewhat higher for a conical gas distributor. In a limited number of cases where extreme infiltration of the buffer layer occurred the discrepancy in buffer thickness was in excess of  $15 \mu\text{m}$ . To determine the effect that the uncertainty in locating the buffer LTI interface introduces into the calculations of buffer density and the corrected immersion density of the LTI, a number of Biso-coating runs were sampled before and after application of the LTI layer. The coating densities obtained with equations not requiring radiograph measurements were compared with coating densities obtained using equations which did. Results for a small fraction of the comparisons that have been made are given in Table 4.

Column 4 of Table 4 gives the corrected immersion density for the LTI layer as determined from Eq. (12) which does not require radiographic measurements. The fifth column contains the corrected immersion density for the LTI layer calculated without any measurements on the buffer coated particles. Comparing Columns 4 and 5 shows that the error in the latter values caused by the uncertainty in the buffer-LTI interface is small ( $0.016 \text{ g/cm}^3$ ). Column six gives the corrected LTI coating density from Eq. (11) with the buffer radiograph being used to determine the buffer coated particle diameter. For these values the error caused by the difficulty in determining the buffer-LTI interface from Biso-coated particle radiographs is avoided. These values agree closely with the values in column 4, lending validity to the use of Eqs. (11) and (12). Similarly, comparisons of buffer density values obtained without radiograph measurements, column 9, with the values of column 10, which were obtained solely from post-LTI data, show that the uncertainty in locating the buffer-LTI interface causes an average error of  $\sim 0.09 \text{ g/cm}^3$  in the latter values. Actually this error is larger than normally encountered since this average includes values for several runs having an

unusually large amount of infiltration. The same comparison when made for 79 coating runs yielded a discrepancy of  $0.077 \text{ g/cm}^3$ . In a production operation one could occasionally measure the magnitude of the shift in the apparent location of the buffer-LTI layer interface and use this value to correct the buffer diameter as read from the Biso radiograph. Such a buffer diameter correction could significantly reduce the uncertainty in the calculated buffer density. Such a correction is usually made (last column of Table 4). The average difference between these values and the values of column 9 is only  $0.036 \text{ g/cm}^3$  which is acceptable. The discrepancy for 79 coating runs averaged  $0.037 \text{ g/cm}^3$ . Such agreement supports the validity of both Eqs. (15) and (23).

Beatty and Weber<sup>13</sup> are developing a technique by which the open pore volume of the buffer layer is measured by high pressure mercury pycnometry performed on crushed samples of fully coated particles. The technique has been demonstrated for particles containing dense  $\text{ThO}_2$  kernels and work is in progress with particles containing porous resin-derived fissile kernels.

### Silicon Carbide Coating Density

Good quality silicon carbide coatings are impermeable to liquids; therefore the geometric density of the SiC layer can be determined by immersing clean SiC fragments in a gradient density column. The liquid column is prepared from two liquids—diiodo methane and a mixture of tetrabromoethane and benzene. Before immersion the fragments are heated to  $900^\circ\text{C}$  in oxygen to remove any adhering carbon. The fragments are then treated with  $13 \text{ M HNO}_3$ — $0.1 \text{ M HF}$  to remove the  $\text{SiO}_2$  formed during the previous heating; otherwise an erroneously low density value will result. Sulfuric acid in the above solution is undesirable since a sulphate residue can often be left on the SiC fragments leading to spurious density values. Before immersion the fragments are dried and then ultrasonically treated with liquid from the gradient column to wet the fragments. Thorough wetting reduces the time required for the fragments to settle to their equilibrium position and improves the precision.

About 15 fragments are used from a given coating run. Usually the variation in density from fragment to fragment is small; the standard deviation is typically  $0.005 \text{ g/cm}^3$  and thus the 95% confidence limit on the mean density for 15 fragments is  $\pm 0.003 \text{ g/cm}^3$ .

### Particle Shape

Most kernel-making processes produce kernels which are essentially spherical and therefore the coated particle shape is primarily controlled by intraparticle nonuniformity of the carbon coating layers (Figs. 2 and 6). A technique has been developed for quantitatively measuring the shape of coated particles.<sup>14</sup> First, the coating thickness on diametrically opposite sides of the particle is measured by microscopic examination of an x-radiograph as previously described on page 5. The index of merit, termed "shape ratio" is obtained by dividing the coating thickness on one side of a particle by the thickness on the opposite side. The larger thickness is always placed in the numerator, so that the shape ratio is greater than unity. The average value obtained from measurements on 50 to 100 particles is used to characterize a particle batch. The comparison of the shape ratio values with the visual appearance shows that the shape ratio is a meaningful measure of particle shape or faceting (Fig. 10). Further evidence that the shape ratio accurately reflects particle shape is that a correlation was shown to exist between shape ratio and particle packing fraction.

---

13. Private communication with R. L. Beatty, Oak Ridge National Laboratory, March, 1976.

14. W. J. Lackey, W. H. Pechin, and J. D. Sease, "Measurement and Control of Shape of Fuel Particles for High Temperature Gas-Cooled Reactors," *Am. Ceram. Soc. Bull.*, 54: 718–24 (August 1975).

Table 4. Comparison of coating densities calculated using equations that do and do not require sampling of the buffer coated particles

Sample	Discrepancy in buffer thickness ( $\mu\text{m}$ )	LTI observed immersion density ( $\text{g}/\text{cm}^3$ )	LTI Corrected Immersion Density, $\text{g}/\text{cm}^3$				Buffer density before LTI deposition ( $\text{g}/\text{cm}^3$ )	Buffer density after LTI deposition, $\text{g}/\text{cm}^3$			
			From Eq (12)	From Eq (11) using Biso radiograph	From Eq (11) using post-LTI data and buffer radiograph	From Eq (11) with $D_B$ corrected $8 \mu\text{m}$		From Eq (15)	From Eq (23) using Biso radiograph	From Eq (23) using post-LTI data and buffer radiograph	From Eq (23) with $D_B$ corrected $8 \mu\text{m}$
(Column 1)	(Column 2)	(Column 3)	(Column 4)	(Column 5)	(Column 6)	Column 7)	(Column 8)	(Column 9)	(Column 10)	(Column 11)	(Column 12)
J-461	9	1.934	1.833	1.841	1.835	1.837	1.106	1.263	1.183	1.243	1.229
J-464	16	1.922	1.828	1.838	1.828	1.834	1.010	1.199	1.080	1.178	1.134
J-469	12	1.966	1.819	1.824	1.813	1.818	1.144	1.315	1.269	1.330	1.310
A-338	17	1.964	1.926	1.929	1.927	1.928	1.240	1.337	1.236	1.287	1.280
A-496	20	2.021	1.938	1.949	1.931	1.945	1.085	1.340	1.275	1.381	1.317
A-498	28	2.030	1.986	1.990	1.986	1.988	1.085	1.323	1.239	1.363	1.285
A-499	26	2.023	1.962	1.970	1.962	1.968	1.085	1.362	1.282	1.399	1.325
A-500	26	1.948	1.783	1.819	1.736	1.802	1.085	1.278	1.219	1.219	1.260
A-501	21	2.021	1.912	1.930	1.913	1.923	1.085	1.335	1.270	1.371	1.312
A-518	10	1.994	1.695	1.717	1.680	1.687	1.326	1.477	1.452	1.494	1.486
A-520	6	1.993	1.871	1.874	1.873	1.871	1.326	1.382	1.370	1.400	1.408
A-522	14	2.009	1.805	1.815	1.797	1.804	1.326	1.375	1.324	1.402	1.369
A-523	2	1.991	1.829	1.832	1.832	1.827	1.326	1.397	1.399	1.411	1.435
A-525	4	1.975	1.661	1.666	1.662	1.634	1.326	1.390	1.388	1.401	1.423
A-593	33	2.040	1.906	1.940	1.905	1.934	0.670	1.507	1.222	1.533	1.322
A-604	16	2.061	1.914	1.945	1.902	1.936	0.981	1.585	1.455	1.594	1.527
A-606	12	2.060	1.918	1.944	1.924	1.934	0.987	1.479	1.328	1.443	1.406
A-608	14	2.045	1.862	1.893	1.868	1.880	1.080	1.347	1.144	1.313	1.248
A-613	17	2.053	1.857	1.887	1.851	1.871	1.040	1.330	1.182	1.358	1.274
Averages	16	2.003	1.858	1.874	1.854	1.864	1.122	1.370	1.280	1.375	1.334

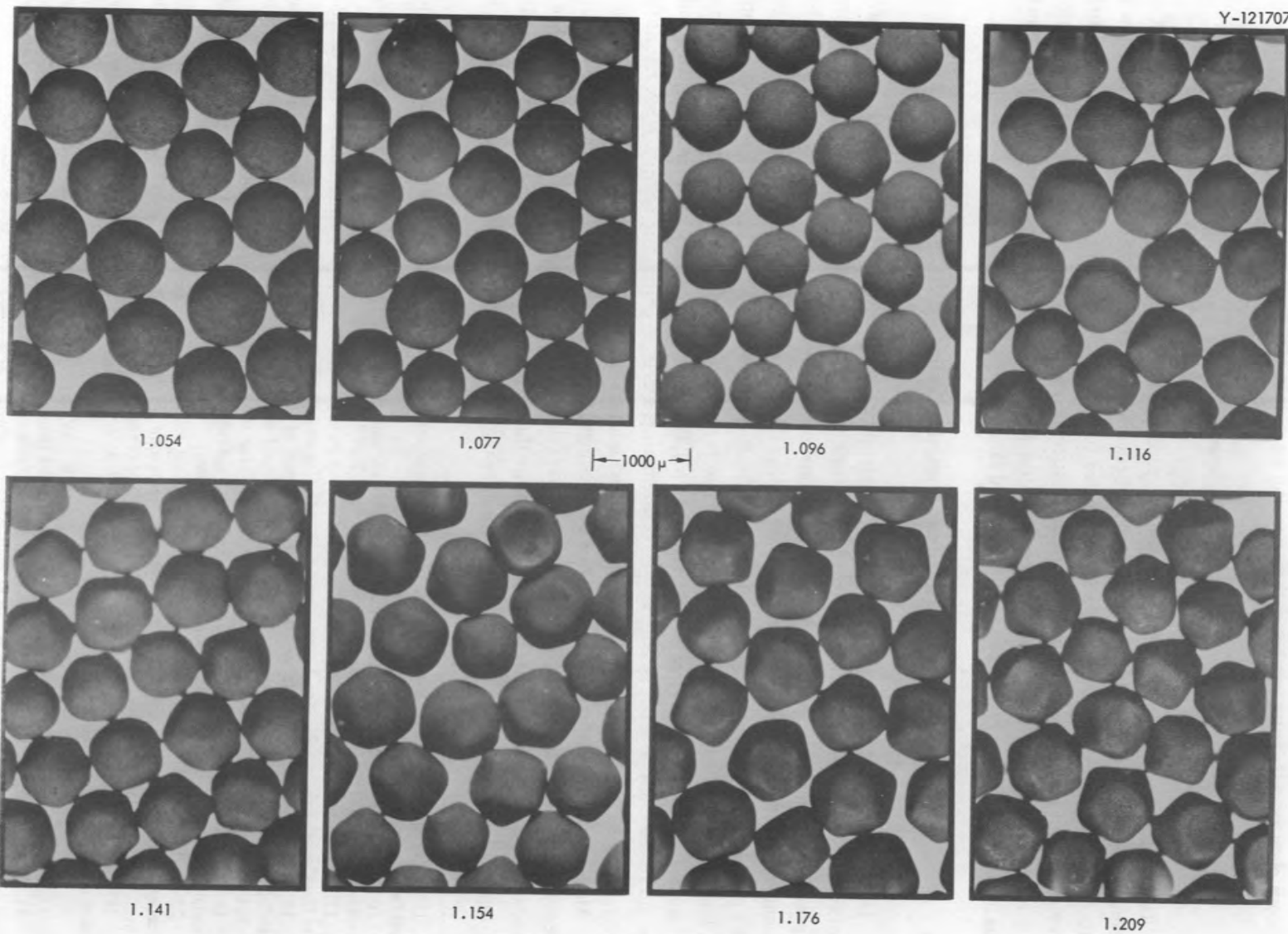


Fig. 10. Comparison of shape ratio with micrographs of Biso-coated  $\text{ThO}_2$ .

Previous experience in measuring and controlling particle shape<sup>14</sup> showed that more nearly spherical particles are obtained with smaller furnace changes, greater gas flow rates, and higher deposition rates. Also, a porous plate gas distributor was better than a conical gas distributor.

### Particle Strength

Techniques have been developed for measuring particle and coating strength.<sup>15-18</sup> A simple test is normally used in which an entire particle is crushed between flat platens. Results from this test indicates a particle's ability to withstand the forces it is subjected to during pneumatic particle transfer and fuel rod fabrication. Our experience<sup>19</sup> with measuring crush strength and the influence of coating process variables on strength showed that 1800°C postcoating anneal for Biso-coated ThO<sub>2</sub> increased particle strength and thus increased the ability of particles to withstand rod fabrication.

### Cracked and Permeable Coatings

Leaching with gaseous chlorine can be used to determine the fraction of Biso-coated particles that have broken or permeable coatings.<sup>20</sup> The technique<sup>21</sup> uses 1500°C gaseous chlorine for 2 hr to remove the exposed heavy metals as volatile chlorides which are then quantitatively recovered and analyzed. This technique works for particles containing Th and/or U in the form of oxide and/or carbide. Use of duplicate 10-g particle samples allows detection of defective fractions of about 10<sup>-4</sup>. Figure 11 is an x-radiograph of leached Biso-coated ThO<sub>2</sub> particles. Note that one kernel has been removed by leaching. The influence of coating thickness and coating process variables on LTI coating permeability has been determined with the aid of the chlorine leach technique.<sup>22,23</sup> Current emphasis is on correlating chlorine leach results for unirradiated fuel with measurements of fission product release from irradiated specimens.

Measurement of the fraction of defective SiC coatings is more difficult and further technique development is needed. Burning to remove the outer LTI layer (also the inner LTI layer if the SiC layer is cracked), followed by aqueous leaching has been used to measure the defective SiC fraction. However, reproducibility of this technique has been poor. An alternate approach<sup>24</sup> consists of burning followed by pressurization in

---

15. K. E. Gilchrist and J. E. Brocklehurst, "A Technique for Measuring the Strength of High Temperature Reactor Fuel Particle Coatings," *J. Nucl. Mater.* 43: 347-50 (1972).

16. K. Bongartz, E., Gyarmati, H. Nickel, H. Schuster, and W. Winter, "Measurement of Young's Modulus and Fracture Stress on HTR Particle Coatings by the Brittle Ring Test," *J. Nucl. Mater.* 45: 261-264 (1972/73).

17. A. G. Evans, C. Padgett, R. W. Davidge, "Strength of Pyrolytic SiC Coatings of Fuel Particles for High-Temperature Gas-Cooled Reactors," *J. Am. Ceram. Soc.* 56: 36-41 (January 1973).

18. P. Krautwasser, H. Nickel, and K. Täuber, "Influence of Microporosity on Fracture Stress of Pyrocarbon Coatings," paper C1/3 in *3rd International Conference on Structural Mechanics in Reactor Technology*, held in London, Sept. 1-5, 1975, Vol. 1, Part C, Comp. by T. A. Jaeger, Commission of the European Communities, Luxembourg, 1975.

19. W. J. Lackey, D. P. Stinton, L. E. Davis, R. L. Beatty, *Crushing Strength of HTGR Fuel Particles*, ORNL-TM-5132 (January 1976). Accepted for publication in *Nuclear Technology*.

20. P. Koss and H. Bildstein, "Fabrication Methods and Evaluation of Uranium-Thorium Carbide Fuel for High-Temperature Gas-Cooled Reactors," in *Proceedings of the Second International Thorium Fuel Cycle Symposium*, Gatlinburg, Tennessee, May 3-6, 1966, p. 253-272. CONF-660524 (February 1968).

21. D. E. LaValle, D. A. Costanzo, W. J. Lackey, and A. J. Caputo, "The Determination of the Defective Particle Fraction in HTGR Fuels" ORNL-TM-5483 (in-press).

22. W. J. Lackey, J. D. Sease, D. A. Costanzo, and D. E. LaValle, "Improved Coating Process for High-Temperature Gas-Cooled Reactor Fuel," *Trans. Am. Nucl. Soc.*, 22: 194-95 (November 1975).

23. G. W. Weber, R. L. Beatty, V. J. Tennery, and W. J. Lackey, "The Effect of Pyrocarbon Coating Permeability on Uranium Redistribution in HTGR Fuels," to be published in *Proceedings of American Vacuum Society, Inc.*

24. D. M. Hewette, II, and W. R. Laing, "Determination of Defective SiC Layers in Coated Nuclear Fuel Particles," *Nucl. Technol.* 21(2): 149-50 (February 1974).

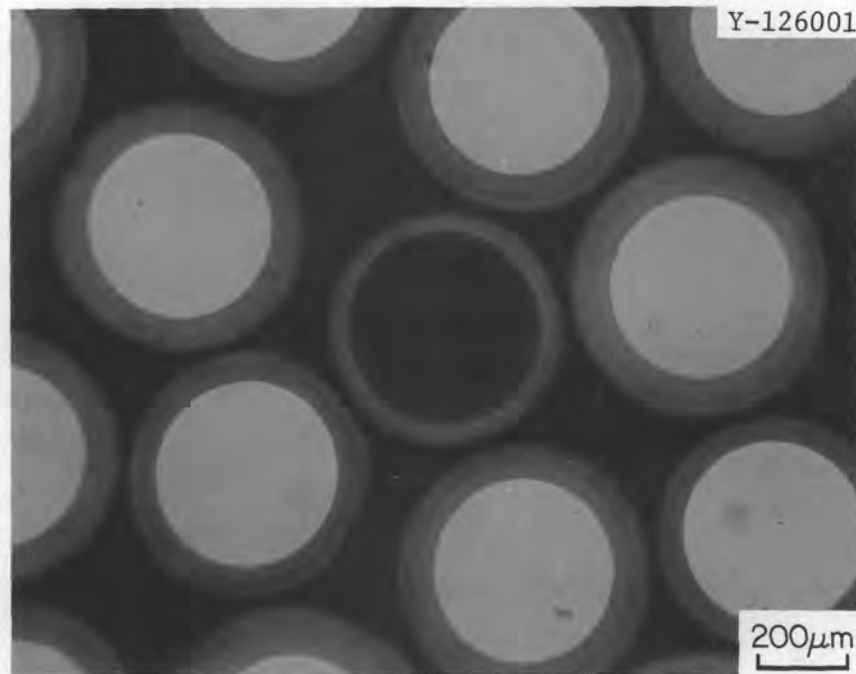


Fig. 11. X-radiograph of chlorine-leached Biso-coated  $\text{ThO}_2$  particles showing one particle from which the  $\text{ThO}_2$  was leached.

103 MPa (15,000 psi) mercury. The particles are then cleaned of surface mercury and radiographed. Particles having cracked SiC layers will contain mercury and so be recognizable in the radiograph.

No quality control technique, other than visual examination for cracks, exists for the outer LTI layer of Triso-coated particles.

#### Kernel and Coating Microstructure

Conventional reflected light microscopy is of value in characterizing HTGR fuel particles (Fig. 12). Kernels and coatings can be checked for unwanted phases as well as for general integrity. Extensive preferred location of soot inclusion or pores in LTI and SiC coatings can lead to an onion-skin-type structure which may lead to in-reactor failure. The frequency of occurrence of pores in SiC coatings is a check, although not a sensitive one, on the SiC density. Visual observation of the reaction of LTI coatings to polarized light is an indication of the degree of preferred orientation. Polarized light also reveals subsurface pores in SiC.

As research tools, the electron microprobe and transmission and scanning electron microscopy are useful. Microprobe analysis has been used with resin-derived kernels to show that the uranium concentration is constant from point-to-point within a given kernel and from kernel-to-kernel. It has also been used to show, (Fig. 13) that in some particles there is uranium in the buffer layer.<sup>25</sup> Scanning electron microscopy is useful for examining coating outer surfaces and fracture surfaces, particularly for SiC. Transmission

25. G. W. Weber, R. L. Beatty, V. J. Tennery, and W. J. Lackey, "Uranium Dispersion in the Coating of Weak-Acid-Resin-Derived HTGR Fuel Microspheres," ORNL/TM-5133 (February 1976).

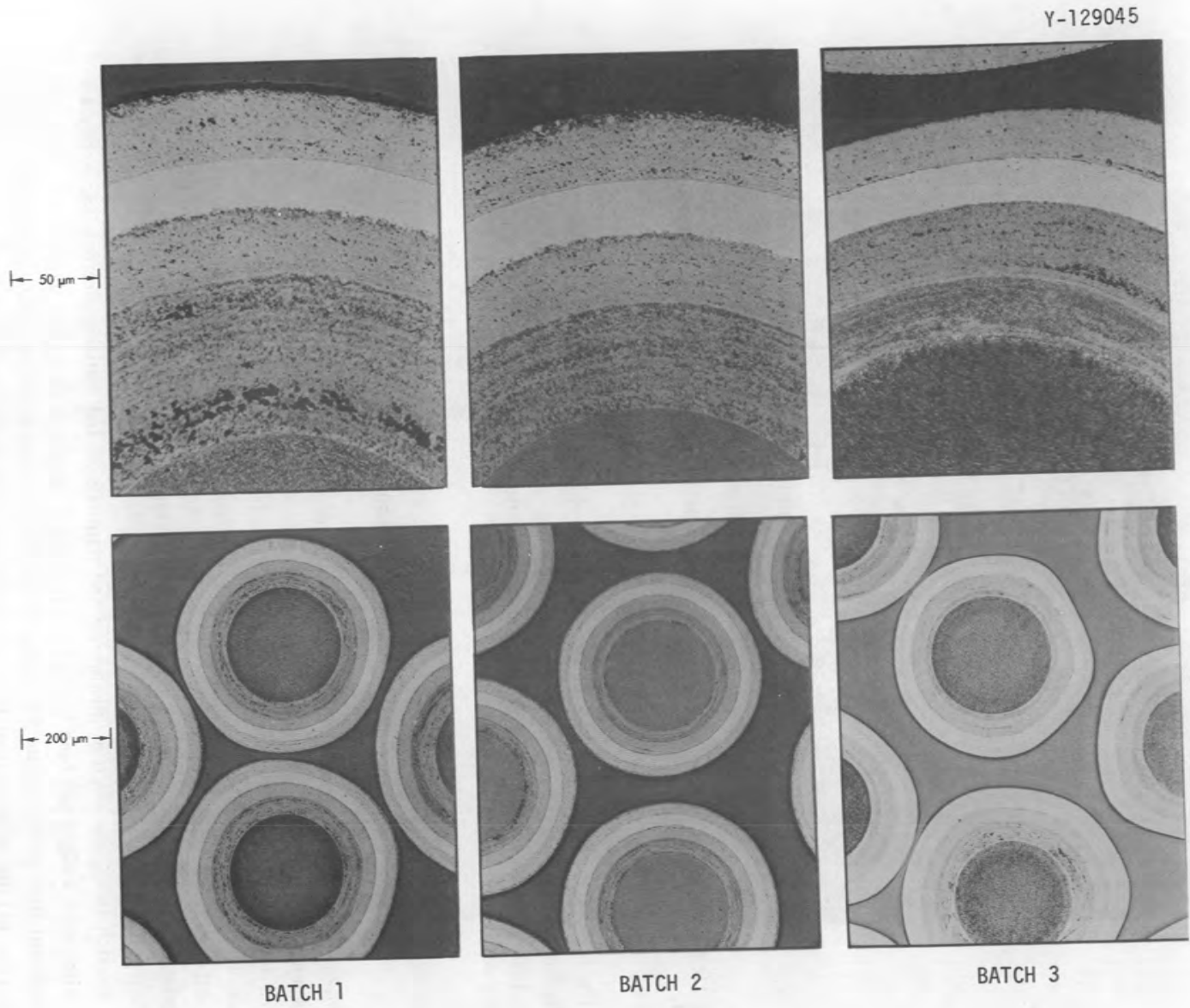


Fig. 12. Micrographs of three batches of Triso-coated 93%  $^{235}\text{U}$ -enriched resin-derived fuel particles. In the top-right micrograph, pores are visible in the SiC layer and a white uranium-bearing phase is visible at the kernel-buffer interface.

electron microscopy of carbon coatings<sup>26-28</sup> helped in formulating models for pyrocarbon deposition and showed that SiC<sup>29</sup> coatings are complex and contain numerous stacking faults. Considerable emphasis has been placed on etching of polished LTI coatings by plasma oxidation.<sup>30-33</sup> This technique yields information which is of some value in predicting coating stability during irradiation.

Three methods have been found useful for etching the SiC coatings. Thermal etching at 1550°C for 30 min in argon has been successful in revealing the grain structure. An electrolytic etchant consisting of a mixture of 500 cm<sup>3</sup> of H<sub>3</sub>PO<sub>4</sub> and 20 g K<sub>2</sub>Cr<sub>2</sub>O<sub>7</sub> used for 1.5 min at a current density of 4 to 5 A/cm<sup>2</sup> etches both large and small grained material to reveal the presence of banding or striations. A third etch<sup>34</sup> involving dipping for 1 to 10 min in a boiling mixture of equal volumes of saturated NaOH and K<sub>3</sub>Fe(CN)<sub>6</sub> water solutions etches both large and small grained material but does not show banding as clearly as does the electrolytic etch. The chemical and thermal etch methods are in close agreement (Fig. 14).

### Coating Anisotropy

The extent to which the c-axes of the LTI layer crystallites are preferentially aligned perpendicular to the substrate is referred to as the Bacon anisotropy factor (BAF)<sup>35</sup> and is pertinent to irradiation induced shrinkage and coating failure. The BAF value can be determined by x-ray diffraction for relatively large disk samples but x-ray methods are difficult to apply to microspheres. Therefore an optical technique is employed to measure the anisotropy of LTI coatings on microspheres.<sup>36,37</sup> More work is needed on any possible influence of coating density on the optically measured BAF value; of annealing and deposition of SiC on the measured BAF value for the inner LTI; and of sample preparation and equipment details on the measured anisotropy value. Also, more work is needed relating anisotropy to coating conditions and defining what anisotropy is suitable for the various LTI layers to provide adequate irradiation performance.

No work has been reported on preferred orientation of SiC crystallites. The influence of this factor as well as other structural features (e.g., grain size) on fission product retention needs to be thoroughly evaluated.

---

26. J. L. Kaae, T. D. Gulden, and S. Liang, "Transmission Electron Microscopy of Pyrolytic Carbons Deposited in a Bed of Fluidized Particles," *Carbon*, 10: 701-709 (1972).

27. J. L. Kaae, "Microstructures of Isotropic Pyrolytic Carbons," *Carbon*, 13: 55-62 (1975).

28. C. S. Yust and H. P. Krautwasser, "Transmission Electron Microscopy of Propene-Derived Pyrolytic Carbon Coatings," *Carbon*, 13: 125-133 (1975).

29. T. D. Gulden, "Stacking Faults in Chemically-Vapor-Deposited Beta Silicon Carbide," *J. Am. Ceram. Soc.*, 54: 498-501 (October, 1971).

30. H. Luhlrich et al., "Determination of the Distribution of Amorphous Regions in Pyrocarbon Coatings by Means of Cold Oxidation," *Z. Anal. Chem.*, 225: 97-103 (1971).

31. K. Bongartz et al., *Improvements in Characterization of Pyrolytic Deposited Carbon*, JÜL-1078-RW (June 1974).

32. H. Luhlrich et al., "Improvements in Characterization Methods of Pyrocarbon," pp. 27-50 in *Quality Control Procedures on Graphite, Pyrocarbon, and Silicon Carbide*, Compiled by K. Koizlik, GERHTR-129, JÜL-1106-RW (September 1974).

33. J. P. Mathers, V. J. Tennery, and E. S. Bomar, *Equipment Variables and Deposition Conditions Affecting the Plasma Oxidation of Pyrocarbon Coatings on HTGR Fuel Particles*, ORNL/TM-5308 (In preparation).

34. Personal communication with J. Holder, C.E.N., Grenoble, France, April 1975.

35. G. E. Bacon, "A Method for Determining the Degree of Orientation of Graphite," *J. Appl. Chem. (London)*, 6: 477-81 (1956).

36. Stevens, D. W., *Optical Anisotropy and Preferred Orientation in Nearly Isotropic Pyrocarbons*, GA-A13307, General Atomic Company, San Diego, California (January 1975), submitted for publication in *Carbon*.

37. Koizlik, K., Tauber, K., Nickel, H. and Wasmund, H., "On the Influence of the Method of Measurement on the Optical Anisotropy Factor OPTAF of Pyrocarbon," JÜL-1082-RW (July 1974); English translation GERHTR-117.

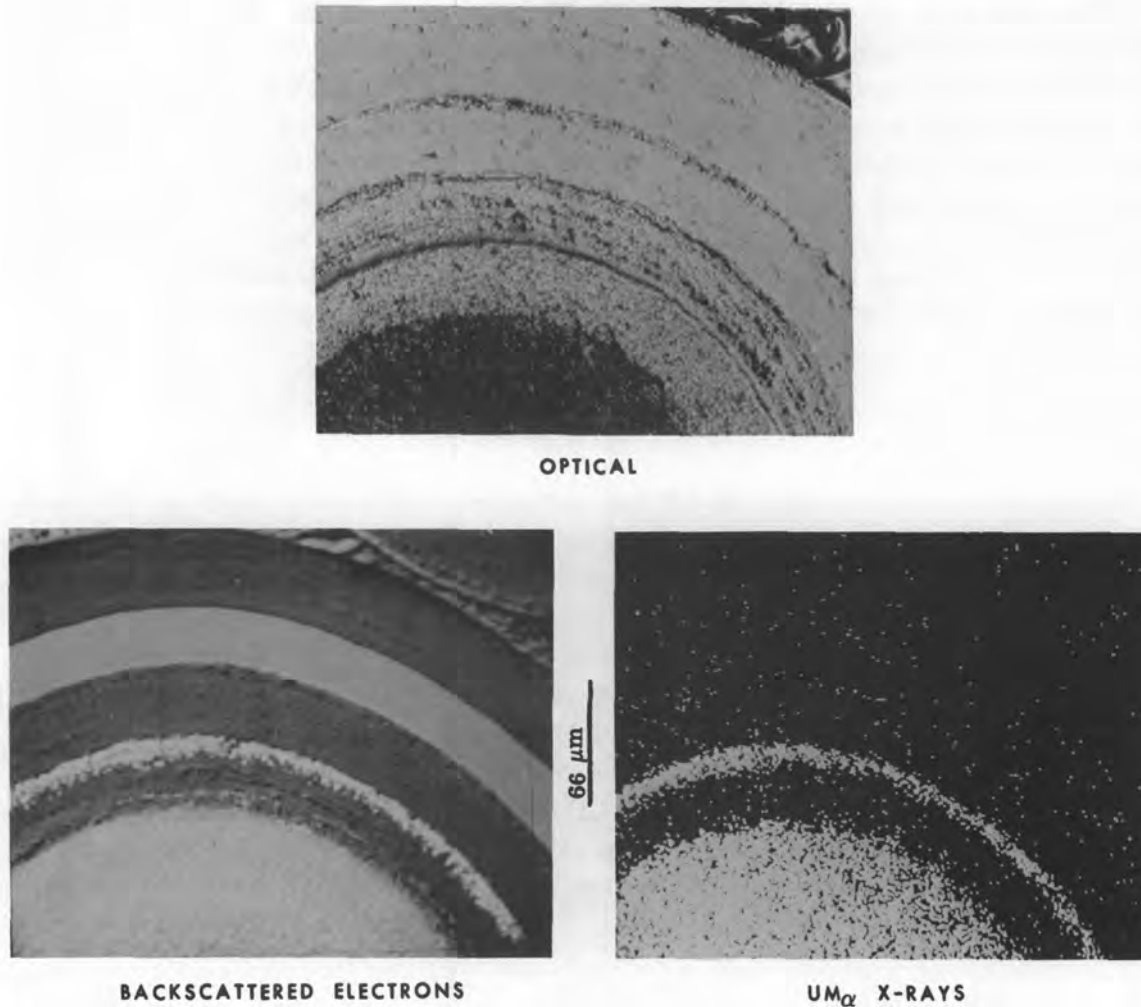


Fig. 13. Uranium distribution in Triso-coated resin-derived fissile fuel particle. Note the band of uranium-bearing material at the buffer-LTI interface. In the  $UM_{\alpha}$  x-ray display (lower right) background accounts for the signals outside the buffer layer.

#### Uranium, Thorium, and Carbon Analysis

The uranium content of uncoated resin derived fissile kernels is determined gravimetrically by combustion in oxygen to  $U_3O_8$ . The carbon content of the kernels is determined by combustion and trapping of the  $CO_2$  in ascarite. The oxygen content of partially converted resin derived kernels is not as accurately measurable as the uranium and carbon contents and the best oxygen values are obtained by difference. When 32 different batches of carbonized or converted resin kernels were each analyzed in duplicate for uranium and carbon, the average difference in the duplicate analyses was 0.29% uranium and 0.13% carbon.

For coated particles, as contrasted to kernels, there is an uncertainty in the uranium content of the sample even for a given number of randomly selected particles, because the kernel size is variable (Fig. 15). For example, given a kernel diameter of  $260 \mu m$  and a kernel volume standard deviation of  $1.87 \times 10^6 \mu m^3$  (corresponds to a diameter standard deviation of  $19 \mu m$ ) then the uncertainty at the 95% level of confi-

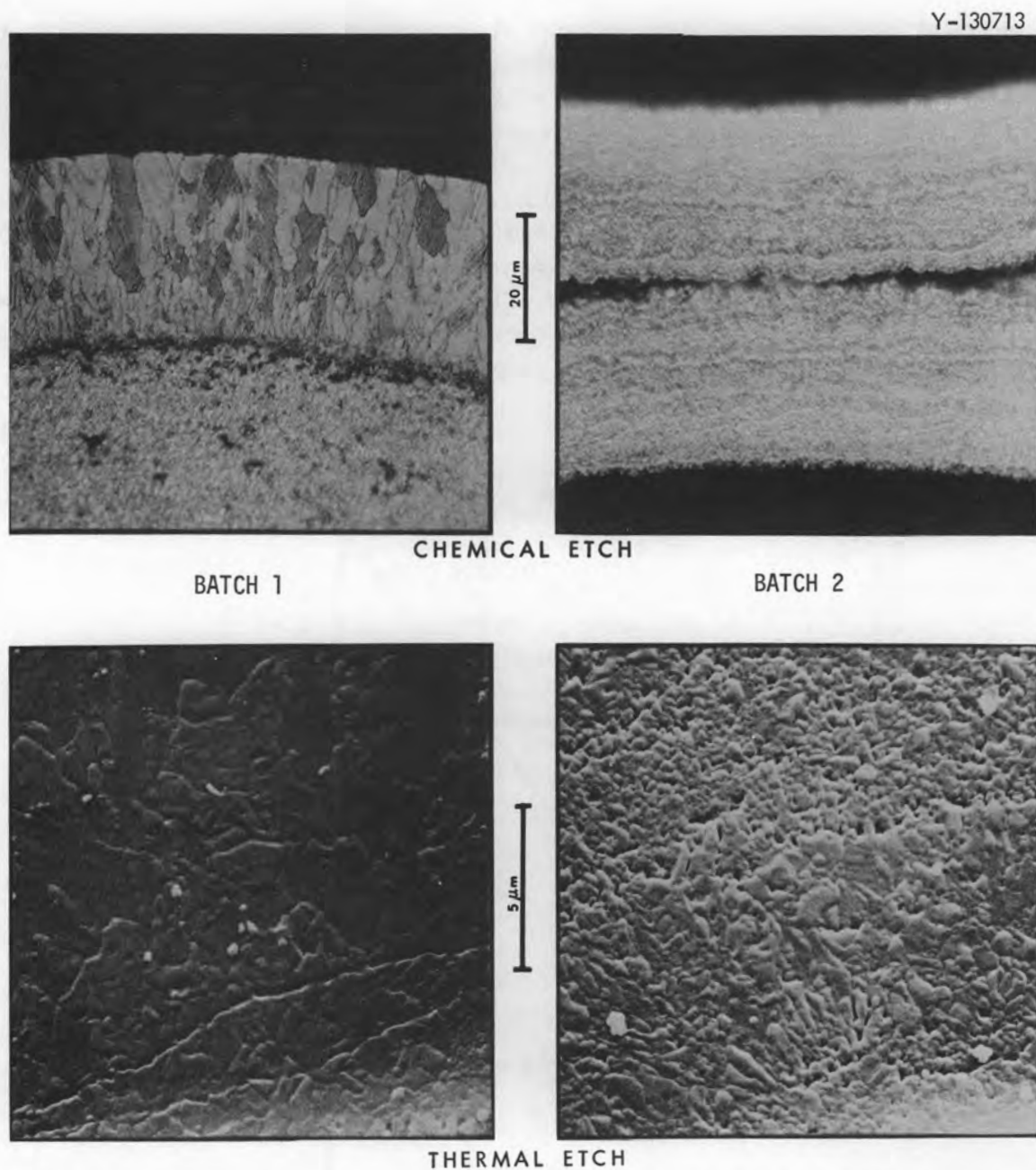


Fig. 14. Grain structure of silicon carbide as revealed by chemical and thermal etching. In the top-left micrograph, the SiC layer and the underlying layer of LTI are visible. The top-right micrograph shows SiC layers from two particles. The fields of view for the bottom two micrographs are within the SiC layer.

dence in the uranium content for a sample consisting of 4825 coated particles (1.0 g of Triso-coated particles) is  $\pm 0.57\%$  of the uranium content. That is, if the actual uranium content of the entire batch were 20%, then at the 95% confidence level the uranium content of the sample of coated particles is within the range  $20 \pm 0.11\%$ . Rather large samples are required to reduce the relative standard deviation to the 0.1% value. Actually, on a weight basis the uncertainty is less than shown in Fig. 15 because, since there is no correlation between coating thickness and kernel diameter, it follows that there will be a correlation between kernel diameter and coating weight. The larger kernels tend to have more coating on a weight basis

and similarly the smaller kernels have less weight of coating on the average. Thus, the uncertainty in uranium content caused by the variation of kernel size is partially compensated. The degree of compensation was determined by a mathematical analysis which considered not only variations in kernel diameter but also typical particle-to-particle variations in coating thickness for each layer of Triso-coated particle (Table 5).

Comparing these data with Fig. 15 shows that the correlation of kernel diameter with coating weight lowers the uncertainty in the uranium content of samples, but this uncertainty is usually the limiting factor in actinide analysis of coated particles unless large samples are used.

The thorium content of carbon-coated  $\text{ThO}_2$  is best determined gravimetrically by burning of the carbon to leave a  $\text{ThO}_2$  residue. The precautions necessary to achieve complete combustion mentioned in the section on as-deposited buffer coating density are applicable.

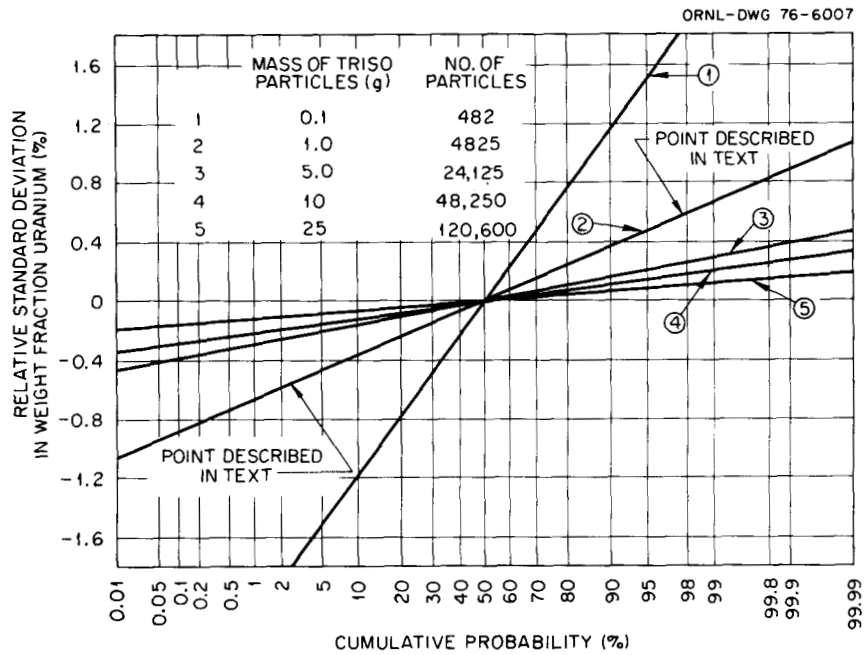


Fig. 15. Uncertainty in uranium content of samples caused by variation in kernel size.

Table 5. Relative standard deviation in the uranium weight fraction of a random sample of Triso-coated particles as a function of sample size

Sample size		Relative standard deviation of uranium weight fraction (%)
Weight (g)	Number of particles	
0.1	482	0.515
1.0	4,825	0.163
5.0	24,125	0.073
10.0	48,250	0.051
15.0	72,400	0.042
25.0	120,600	0.033

The determination of uranium in Triso-coated fissile particles is difficult because of the chemically inert SiC coating. Three methods have been used to convert Triso-coated particle samples to a solution form amenable to uranium measurement.

One method involves ignition at 1000°C in air to remove the outer pyrocarbon layer, fusion of the intact SiC-coated particles with sodium carbonate, dissolution of the melt in nitric acid, and filtration of the sample solution to remove silica. If carbon is present in the residue, the filter paper and residue are wet ashed with a mixture of perchloric acid-nitric acid, the solution filtered and the filtrate combined with the bulk sample solution for measurement.

A second method involves crushing the sample, ignition at 1000°C to remove the pyrocarbon layers, leaching of the ignition residue with 13 *M* HNO<sub>3</sub>–0.1 *M* HF, and filtration to remove the insoluble SiC residue. Since a small amount of uranium (~0.1–0.3 wt %) is associated with the SiC, the SiC residue is fused with Na<sub>2</sub>CO<sub>3</sub> and the melt analyzed for uranium.

A third method involves sequential treatment of the sample with oxygen, chlorine and oxygen at 1000°C to remove the pyrocarbon and silicon carbide coatings. The oxide residue that remains is then dissolved in nitric acid. This method of sample preparation is quicker than the fusion or grind-leach method, 8 hr vs 24–36 hr, respectively. This method is advantageous for glove box and hot-cell operation because the treatment with oxygen and chlorine and the acid dissolution can be performed in a single reaction apparatus.

The precise measurement of uranium in the nitric acid is made by the Davise-Gray method in which the uranium is first reduced with ferrous sulfate and then titrated potentiometrically with dichromate. The relative standard deviation for the precision of this method has been established at 0.05%.

### Impurity Analysis

Trace impurities in coated particles are best determined by spark source mass spectrometry. The samples are crushed in a hard-chrome-plated mortar and pestle to prevent the pickup of impurities other than chromium. The crushed sample is mixed with silver powder and pressed into a pellet which serves as the electrode. Plastic ware is used in the preparation of pellets to further minimize sample contamination.

### FUEL RODS

Fuel rods 13 or 16 mm ( $\frac{1}{2}$  or  $\frac{5}{8}$  in.) in diameter and 50 to 65 mm (2–2.5 in.) long contain mixtures of fissile, fertile and graphite shim particles bonded by a matrix of pitch binder and graphite filler. A large HTGR core contains about  $9 \times 10^6$  rods. The principal activities in the reference recycle fuel rod fabrication process are dispensing, blending, and loading particles into molds; injecting the matrix into a bed of particles to form a fuel rod; and inspecting. In addition to describing a system for fuel rod transfer, this section deals with two important rod attributes – actinide content and homogeneity.

### Fuel Rod Transfer

Fired and unfired fuel rods must be transferred out of the hot cell to various sample inspection stations. A system has been designed to load the rods into capsules, vacuum transfer the rods to a receiving station, unload the rods, and return the capsules. The method chosen for loading and unloading the rods uses a hollow capsule with “collars” inside each end for trapping spherical end plugs. A force of only 4.4 N (1 lb) is required to push the resilient ball plugs into and out of the capsule. The capsules were conveyed at about

6 m/sec (20 fps) in 25-mm-diam (1 in.) tubing 21-m (70 ft) long with an air flow of 3.8 std liters/sec (8 scfm) at a pressure differential of 1.7 kPa (7 in. water). Bends made on a 0.46-m (18 in.) radius have posed no problems and a 0.6-m (2 ft) dead air column is sufficient cushioning to receive the capsule.

### Uranium Content

A nondestructive uranium assay instrument currently under development for HTGR fuel rods will use a  $^{252}\text{Cf}$  neutron source to irradiate the uncarbonized fuel rods. The neutrons induce fission in the fissile material, and the resulting prompt fission neutrons are detected with  $^4\text{He}$ -filled proportional counters. The detected count rate is directly related to the fissile content and can be calibrated with rods of known uranium loadings. An advantage of this approach is that the fast neutron detectors can be made insensitive to gamma radiation. The high gamma activity of the recycled fuel precludes the application of many nondestructive assay techniques presently developed for light-water-reactor fuel or  $^{235}\text{U}$ -Th HTGR fuel. The active  $^{252}\text{Cf}$  assay method was selected after a study<sup>38,39</sup> of HTGR fuel characteristics and their effect on nondestructive assay techniques.

The assay development program at ORNL is directed towards operation of an engineering-scale assay instrument for  $^{233}\text{U}$ -loaded fuel rods. The assay instrument must be remotely operable and maintainable so as to function in-line in a commercial refabrication facility. The program to develop this capability began with the design and fabrication of a laboratory-scale system to optimize the characteristics of a prototypic assay instrument (Fig. 16). A 1.4-mg  $^{252}\text{Cf}$  source is positioned at the center of a cylindrical moderator assembly composed of graphite, polyethylene, and heavy water. The fuel rods are positioned along the periphery of the moderator assembly. In this position they are exposed to well-thermalized neutrons, which selectively fission only the  $^{233}\text{U}$  or  $^{235}\text{U}$  atoms within the rods. The fission neutron detector which is a  $^4\text{He}$  proportional counter, records the number of prompt fission neutrons emitted from the sample. The calculated response function of this device has been previously reported.<sup>38</sup>

For the chemical determination of thorium and uranium in a green rod containing fissile and fertile particles, the rod is refluxed in pyridine to dissolve the pitch binder, and the particles are separated from insoluble matrix debris by filtration. The sample is then prepared for thorium and uranium measurement, as previously described for fissile particles. The thorium in the solvent has been determined by precipitation as the oxalate and gravimetric measurement as  $\text{ThO}_2$ ; the thorium has also been determined volumetrically by titration with ethylenediaminetetraacetic acid.

For the analysis of a fired fuel rod, the sample is ignited at  $1000^\circ\text{C}$  and the thoria kernels and silicon carbide coated fissile particles treated in the manner described for fissile particle sample preparation.

### Actinide Homogeneity

Sectioning of a fuel rod followed by chemical analysis is one method for determining whether the actinides are uniformly distributed throughout the rod. However, this technique is time consuming and expensive, particularly for recycle fuel. Consequently, an effort is underway to develop a nondestructive

---

38. J. D. Jenkins, S. R. McNeany, and J. E. Rushton, *Conceptual Design of the Special Nuclear Material Nondestructive Assay and Accountability System for the HTGR Fuel Refabrication Pilot Plant*, ORNL-TM-4917 (July 1975).

39. J. E. Rushton, J. D. Jenkins, and S. R. McNeany, "Nondestructive Assay Techniques for Recycled  $^{233}\text{U}$  Fuel for High-Temperature Gas-Cooled Reactors," *J. Inst. Nucl. Mater. Management*, 4(1): 18-35 (Spring 1975).

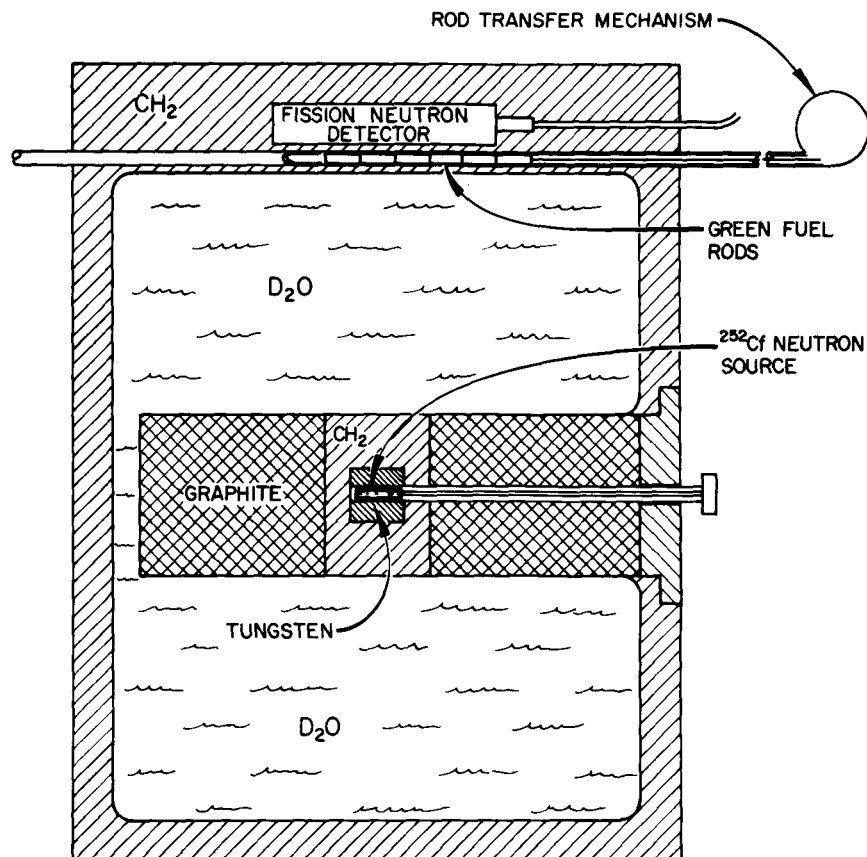


Fig. 16. HTGR fuel assay development device prompt fission neutron configuration.

method for measuring fuel rod homogeneity. Approaches which have been evaluated are x-ray attenuation, gamma-ray attenuation, passive counting of emission from radioactive isotopes present in fuel rods, nuclear magnetic resonance, and x-ray fluorescence. The feasibility of x-ray attenuation has been demonstrated for determining the axial heavy metal homogeneity and the possibility of determining radial homogeneity by this method is being studied.

The use of multiple radioisotopes as gamma-ray sources for determining total heavy metal, total mass, uranium, thorium, and light-element content and relative distribution in fuel rods is being evaluated. A radioisotope source would be advantageous to use in a hot cell environment, since high-voltage power lines, x-ray vacuum tubes, and cooling systems are not required. In addition, the discrete gamma-ray energies simplify the analyses and can yield additional information as to the elemental mass distribution in fuel rods.

### FUEL ELEMENTS

The portion of fuel element fabrication which must be performed remotely consists of the following: (1) loading of the green (unfired) fuel rods into the fuel element block, (2) heating the assembly to about  $1000^\circ\text{C}$  to carbonize the pitch binder of the rods, (3) annealing at  $1800^\circ\text{C}$  to remove residual volatiles and stabilize fuel rod dimensions, (4) loading of poison rods into the element, (5) loading and cementing into place the graphite fuel hole plugs and dowels, and (6) inspecting the fuel element.

### Exposed Actinide

Since particle coatings can crack from the forces present during fuel rod molding, carbonization, and annealing, it is important to measure the fraction of actinide not contained within intact coatings for the final fuel element. Since testing of an entire element is not practical samples processed along with the element must be evaluated. The chlorine leach technique previously described for coated particles has been modified for this purpose. The chlorine passes through a quartz tube supporting a hollow graphite tube, which holds the inductively heated sample. A flow of chlorine through the approximately 20%-porous fuel rod is achieved by packing the rod snugly in the holder with porous carbon particles. Typically a 2 hrs treatment at 1500°C removes 96% of the exposed thorium. Additional development is needed since this technique would not detect Triso-coated particles having defective SiC layers provided either the inner or outer LTI layer was intact.

The pore size distribution of the fuel rod matrix is important for three reasons: An excessive amount of macroporosity (>50  $\mu\text{m}$  diam) reduces fuel rod integrity. (An allowable range is specified for the amount of microporosity.) Excess microporosity lowers the matrix thermal conductivity while too little microporosity can result in a matrix which is too strong which can lead to tearing of LTI outer coating layers during carbonization, annealing, and irradiation. Matrix pore size distributions are measured on polished rod crosssections using commercially available quantitative image analyzing systems.

Other fuel element attributes requiring measurement are pressure drop of coolant passages, surface contamination, and mechanical integrity. Ultrasonic techniques may be suitable for measuring element integrity.

### CONCLUSIONS AND RECOMMENDATIONS

1. High radiation levels require that sample inspection be performed in shielded glove boxes with automated sample handling and analysis equipment.
2. Means for obtaining and transferring representative particle and rod samples have been developed.
3. Precise methods have been developed and demonstrated for measuring buffer coating density after application of the LTI layer and for measuring the geometric density of LTI coatings.
4. Useful techniques exist for the measurement of particle shape and strength.
5. The chlorine leach technique is useful for determining the fraction of defective Biso-coated particles but additional development is needed for Triso-coated particles.
6. Important areas requiring further development are coating anisotropy, correlation of SiC properties with fission product release rates, nondestructive assay, measurement of fuel rod homogeneity, and most fuel element inspections.
7. As a matter of philosophy, inspections performed in support of initial and recycle fuel fabrication development activities and inspection of fuel fabricated for irradiation testing should be extensive. Practically every possible characterization technique should be used so that a thorough understanding of individual fuel properties and property correlations can be made. On the other hand, a major consideration in development of inspection techniques for future commercial production operations is that the fabrication process should be interrupted as little as possible. For example, it is undesirable to interrupt the coating process after the application of each coating layer; the goal in particle characterization is to be able to adequately characterize particles given only a sample of the completely coated particles.

## APPENDIX A

SYMBOLS USED FOR DERIVATION OF EQUATION (23) FOR CALCULATING  
BUFFER DENSITY AFTER APPLICATION OF THE LTI LAYER

$\rho_B$  = Corrected density of buffer coating after application of the LTI layer, g/cm<sup>3</sup>.

$\rho_K$  = Geometric density of kernel, g/cm<sup>3</sup>.

$f$  = Weight fraction carbon in Biso-coated particle.

$\rho_L$  = Geometric density of Biso-coated particles obtained at low pressure mercury, g/cm<sup>3</sup>.

$\rho_C$  = Corrected immersion density (geometric density) of LTI coating, g/cm<sup>3</sup>.

$D_K$  = Diameter of kernel, cm.

$D_B$  = Diameter of buffer coated particle, cm.

$D_L$  = Diameter of LTI coated particle, cm.

$R_1$  = Average value for  $n$  particles of the ratio of the volume of the buffer coated particle to the kernel volume

$$= \frac{\sum_{i=1}^n (D_{B_i}/D_{K_i})^3}{n}$$

This quantity is given sufficiently accurately for values of  $n \approx 50$  to 200 by cubing the value obtained when the average diameter of the buffer coated particle is divided by the average kernel diameter, that is,  $(\bar{D}_B/\bar{D}_K)^3$ .

$R_2$  = Average value for the ratio of the volume of the LTI coated particle to the kernel volume for  $n$  particles,

$$= \frac{\sum_{i=1}^n (D_{L_i}/D_{K_i})^3}{n}$$

## ACKNOWLEDGMENTS

The authors express their thanks to the numerous people who made this work possible. In particular, the assistance of R. L. Beatty, D. P. Stinton, C. E. DeVore, and J. B. Flynn in the preparation and characterization of coated particles was invaluable. R. R. Suchomel and M. G. Willey are thanked for their efforts in developing the particle samplers, and J. E. Mack and D. R. Johnson were responsible for the particle and rod transfer studies. J. E. Rushton did the dose rate calculations, and R. W. Knoll analyzed the influence of varying kernel size and coating thickness on the precision of uranium analyses. J. E. Mack and L. J. Turner played major roles in development of the particle size analyzer. Many weeks of work was performed by D. A. Costanzo, J. L. Botts, L. J. Brady, W. R. Laing, D. E. LaValle, and F. R. Layton in developing and using the analytical chemistry techniques. The work dealing with fuel rods was performed by P. Angelini, R. A. Bradley, A. J. Caputo, and D. R. Johnson. J. D. Jenkins, S. R. McNeany, and J. E. Rushton were responsible for nondestructive uranium assay. Metallography was performed under the direction of R. J. Gray and B. C. Leslie. The manuscript was edited by George Griffith and prepared for publication by the Metals and Ceramics Division Reports Office.



*INTERNAL DISTRIBUTION*

- |                                     |                                     |
|-------------------------------------|-------------------------------------|
| 1-3. Central Research Library       | 57. J. E. Mack                      |
| 4. Document Reference Section       | 58. C. J. McHargue                  |
| 5-14. Laboratory Records Department | 59. S. R. McNeany                   |
| 15. Laboratory Records, ORNL R.C.   | 60. C. S. Morgan                    |
| 16. ORNL Patent Office              | 61. M. T. Morgan                    |
| 17. P. Angelini                     | 62. K. J. Notz                      |
| 18. R. L. Beatty                    | 63. A. R. Olsen                     |
| 19. R. A. Bradley                   | 64. P. Patriarca                    |
| 20. A. J. Caputo                    | 65-69. W. H. Pechin                 |
| 21. J. A. Carpenter                 | 70. H. Postma                       |
| 22. J. H. Coobs                     | 71. J. M. Robbins                   |
| 23. D. A. Costanzo                  | 72. J. E. Rushton                   |
| 24. F. L. Culler                    | 73. J. D. Sease                     |
| 25. J. E. Cunningham                | 74. J. H. Shaffer                   |
| 26. C. E. DeVore                    | 75. D. P. Stinton                   |
| 27. R. G. Donnelly                  | 76. R. R. Suchomel                  |
| 28-32. W. P. Eatherly               | 77. V. J. Tennery                   |
| 33. J. I. Federer                   | 78. S. M. Tieg                      |
| 34. J. B. Flynn                     | 79. T. N. Tieg                      |
| 35. P. A. Haas                      | 80. D. B. Trauger                   |
| 36. R. L. Hamner                    | 81. G. W. Weber                     |
| 37. R. F. Hibbs                     | 82. J. R. Weir, Jr.                 |
| 38-40. M. R. Hill                   | 83. M. G. Willey                    |
| 41. F. J. Homan                     | 84. R. G. Wymer                     |
| 42. J. D. Jenkins                   | 85. R. M. Young                     |
| 43. D. R. Johnson                   | 86. C. S. Yust                      |
| 44. M. J. Kania                     | 87. R. W. Balluffi (consultant)     |
| 45-46. P. R. Kasten                 | 88. P. M. Brister (consultant)      |
| 47-51. W. J. Lackey                 | 89. W. R. Hibbard, Jr. (consultant) |
| 52. D. E. LaValle                   | 90. Hayne Palmour III (consultant)  |
| 53. T. B. Lindemer                  | 91. N. E. Promisel (consultant)     |
| 54. E. L. Long, Jr.                 | 92. D. F. Stein (consultant)        |
| 55-56. A. L. Lotts                  |                                     |

*EXTERNAL DISTRIBUTION*

- 93-100. ERDA DIVISION OF NUCLEAR FUEL CYCLE AND PRODUCTION, Washington, DC 20545  
 Director (2)  
 R. G. Bradley (1)  
 W. S. Schieb (5)
- 101-102. ERDA DIVISION OF REACTOR NUCLEAR RESEARCH AND APPLICATIONS, Washington, DC 20545  
 Director
- 103-104. ERDA IDAHO OPERATIONS OFFICE, P.O. Box 2108, Idaho Falls, ID 83401  
 C. E. Williams, Manager  
 Barry Smith

105. ERDA OFFICE OF PROGRAM MANAGEMENT, RESEARCH AND SPACE PROGRAMS, P.O.  
Box 81325, San Diego, CA 92138  
J. B. Radcliffe
106. ERDA SAN FRANCISCO OPERATIONS OFFICE, 1333 Broadway, Wells Fargo Bldg., Oak-  
land, CA 94612  
R. D. Thorne, Manager
- 107–108. ERDA OAK RIDGE OPERATIONS OFFICE, P.O. Box E, Oak Ridge, TN 37830  
Director, Research and Technical Support Division  
Director, Reactor Division  
F. E. Dearing, Reactor Division
- 109–285. ERDA TECHNICAL INFORMATION CENTER, P.O. Box 62, Oak Ridge, TN 37830  
For distribution as shown in TID-4500 Distribution Category,  
UC-77 – Gas-Cooled Reactor Technology
- 286–293. Copies – ERDA Exchange Agreements with Germany and Dragon Project